Max-Planck-Institut
für Meteorologie

REPORT No. 148

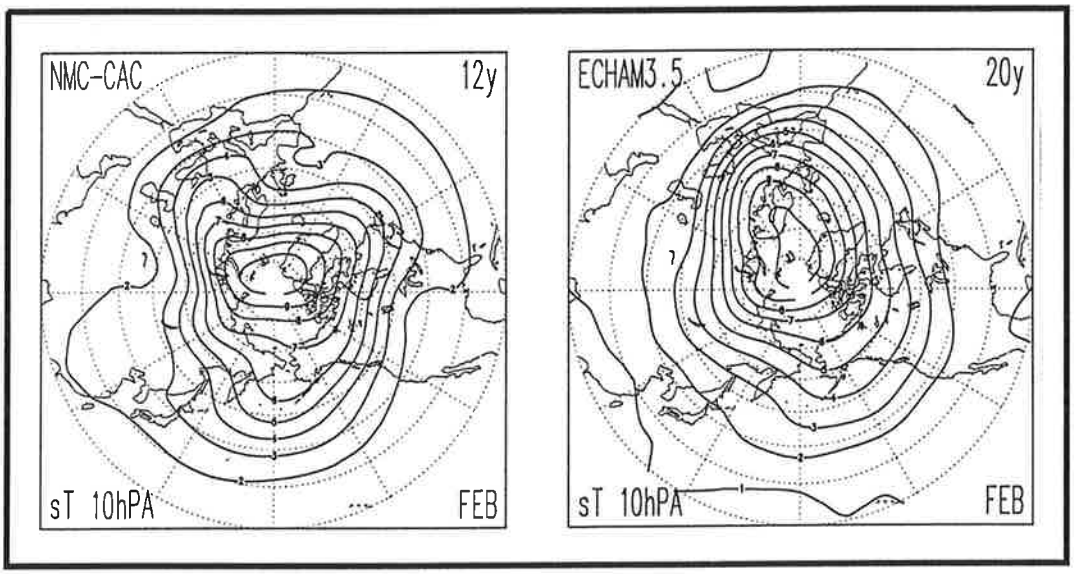

STRATOSPHERIC CLIMATE AND VARIABILITY FROM A GENERAL CIRCULATION MODEL AND OBSERVATIONS. PART I : RESULTS FOR THE DECEMBER-FEBRUARY SEASON.

by

ELISA MANZINI • LENNART BENGTSSON

HAMBURG, November 1994

AUTHORS:

Elisa Manzini
Lennart Bengtsson

Max-Planck-Institut
für Meteorologie

MAX-PLANCK-INSTITUT
FÜR METEOROLOGIE
BUNDESSTRASSE 55
D-20146 Hamburg
F.R. GERMANY

Tel.: +49-(0)40-4 11 73-0
Telefax: +49-(0)40-4 11 73-298
E-Mail: <name> @ dkrz.d400.de

ISSN 0937–1060

Stratospheric climate and variability from a general circulation model and observations. Part I: Results for the December-February season.

Elisa Manzini and Lennart Bengtsson
Max Planck Institute for Meteorology
Hamburg, Germany

Abstract

The climate and variability of the large scale stratospheric circulation during the Northern Hemisphere winter are studied comparing atmospheric statistics from a model simulation and from global observations. The simulation consisted of a 20-year integration performed with a newly developed comprehensive, low resolution model of the troposphere and stratosphere. The observations were compiled by Randel (1992) from a 12-year dataset of NMC-CAC global operational analyses of the troposphere and stratosphere.

The December-February time average of the observed zonal mean circulation is found to be reasonably well captured by the model. In the stratosphere, the magnitude of the simulated and observed zonal winds compares well, although the simulated westerly winds do not show the equatorward tilt with height present in the observations. Associated with the polar confinement of the westerly winds is a relatively small systematic cold bias in the polar lower stratosphere and upper troposphere. The quasi-stationary planetary waves are also well captured by the long term time averaged fields of the model.

A considerable amount of monthly interannual variability is also found in the simulation. Both the NMC-CAC and model datasets show that in the stratosphere the interannual variability increases from December to January and February. The magnitude of the simulated interannual variability compares well with that observed during January and February. In December, however, the interannual variability simulated by the model appears to be severely underestimated in the upper troposphere and, locally, in the lower stratosphere.

During February substantially different results were obtained when the monthly interannual variability was computed from 10-year samples of the simulation. This behavior appeared to be caused by the occurrence of two major warming type events during the first ten Februaries of the 20-year simulation, while none during the second ten Februaries, a result not in disagreement with observations. The fact that significant differences can occur for 10-year samples indicates that much longer integrations would be necessary for any firm conclusion concerning interannual variability.

1. Introduction

Long term global observations and model simulations are necessary to investigate the nature of climate variability on interannual time scales. Most of the literature on this subject focused mainly on the tropospheric flow and its response to changes in boundary forcing, namely variations in sea surface temperature and land parameters (for a review see for instance Lau, 1992).

Recently it has been recognized that anthropogenic influences of the atmospheric composition may have a large impact on the stratosphere, a dramatic example being the rapid depletion of the ozone layer during the austral spring over Antarctica (Farman et al. 1985). Significant ozone losses in the middle and high latitudes of the lower stratosphere (Stolarski et al., 1991) may also affect the climate radiative forcing of the surface-troposphere system (Ramaswamy et al.,1992). However, in order to evaluate the effects of changes in atmospheric composition on the general circulation it is necessary to take into account the large interannual variability of the stratospheric flow. Well known examples of variability in the stratosphere are the so called sudden warmings of the winter polar temperature, that may be particularly intense in the Northern Hemisphere, and the quasi-biennial oscillation in the zonal wind in the lower tropical stratosphere (Andrews et al., 1987 for a review). The complicated interactions among chemistry, radiation and dynamics that appear to characterize the middle atmosphere have therefore motivated and renewed the interest in the climate of the stratosphere and its variability. In addition, availability of relatively long records of global observations including the stratosphere and more advanced numerical models now allow to address this issue more comprehensively.

In this study, the climate of the stratosphere and its variability is investigated by analyzing a 20-year simulation performed with a newly developed General Circulation Model (GCM). The statistics generated by this simulation are thereafter compared with that of a 12-year dataset of global observations of the troposphere and stratosphere (Randel, 1992). Attention is restricted to interannual variability associated with internal dynamical and physical processes, therefore such external forcing as interannual variations in sea surface temperature and in trace gases have been excluded from the simulation. This approach is motivated by the important role played by GCMs in studying the nature of climate variability and thus the necessity of assessing the amount of variability generated in a model atmosphere in the absence of external forcing. The present work is part of a more general project aimed at developing and validating a GCM to be used in a variety of applications.

Previous studies of stratospheric climate and variability simulated by general circulation models include the works of Boville and Randel (1986), Rind et al. (1988a,b), Hamilton et al. (1994) and Hamilton (1994). Boville and Randel (1986) compared the atmospheric

statistics of a 7-year January dataset of global observations to a January perpetual integration obtained with the NCAR-CCM0 general circulation model. About the interannual variability of the stratospheric circulation, they found that their simulation overestimated the observed variability. They attributed their results to the absence of the seasonal cycle in their simulation. The 5-year integration of Rind et al. (1988a,b) performed with the GISS global climate model that included the middle atmosphere suggested that complex interactions among the mean flow, large scale eddies and parametrized gravity wave drag can affect the simulation of the interannual variability in the stratosphere. Very recently, a statistical analysis of several aspects of the climate and variability simulated by the GFDL SKYHI general circulation model of the troposphere stratosphere and mesosphere has been recently completed (Hamilton et al. 1994, Hamilton, 1994). In a 25-year integrations, the Hamilton (1994) results showed that a reasonable amount of daily and interannual variability is present in the SKYHI model during the Northern Hemisphere winter.

The focus of the current work is on evaluating against available observations the model generated long term time average and interannual variability of the monthly mean circulation during December, January and February. Given the generally low variability during the summer season in the stratosphere, the results presented will mainly cover the Northern Hemisphere (NH). Results from the other months of the year as well as analyses of daily variability will be reported in a later study.

The paper is organized as follow. Section 2 describes the troposphere - stratosphere general circulation model and the design of the experiment. The global observation dataset used is introduced in Section 3. Aspects of the simulation of the midlatitude tropospheric circulation of interest to the present contest are summarized in section 4. The long-term time average and the interannual variability of the zonal mean circulation are reported Section 5. Section 6 deals with quasi - stationary planetary waves. Conclusions are discussed in Section 7.

2. The model and the experiment design

The model used in this work is an modified version (hereafter referred to as ECHAM3.5) of the ECHAM3 model described in Roeckner et al. (1992). ECHAM3 is a general circulation spectral transform model with variable horizontal truncation.

The physical parametrizations common to both ECHAM3 and ECHAM3.5 are the following: prognostic scheme for stratiform clouds (Roeckner et al. 1991); cumulus and stratocumulos convection (a mass flux scheme including deep, midlevel and shallow convection, Tiedtke, 1989); standard local vertical diffusion (Louis, 1979) revised to include cloud water effects and non-zero above the planetary boundary layer for unstable stratification only (Roeckner et al. 1992); planetary boundary layer (Louis,

1979); three layer model of heat conduction and soil model (Blondin, 1989; Dümenil and Todini, 1992).

Some of the modifications to the ECHAM3 model included in this work are part of a project aimed at developing the cycle-4 of the ECHAM general circulation models. The modifications included in the ECHAM3.5 model are here summarized:

(i) A new vertical structure of the hybrid sigma-pressure vertical coordinate used in ECHAM3. The model top was raised from the original 10 hPa (middle stratosphere) to 0.1 hPa (middle mesosphere) and the number of vertical levels was increased from 19 to 35. Particular care was taken to ensure a smooth decrease in resolution with height and a resolution slightly higher than that in ECHAM3 near the tropopause (about 1.5 km instead of about 2 km in ECHAM3). The ECHAM3 vertical structure is therefore maintained from the surface to 500 hPa only, while above 500 hPa a finer resolution is used. The vertical structures of ECHAM3 and ECHAM3.5 are compared in Fig. 1.

(ii) A semi-Lagrangian transport scheme (Rasch and Williamson, 1990) for water vapor and cloud water. This scheme substitutes the previous Eulerian horizontal and vertical advection of cloud water and water vapor. With the introduction of the semi-Lagrangian transport, horizontal diffusion of cloud water and water vapor was also eliminated, while vertical diffusion was kept. The behavior of the semi-Lagrangian scheme was validated by E. Roeckner.

(iii) A radiation scheme (Morcrette, 1991) aimed at being flexible to the introduction of exotic trace gases and aerosols and being able to take into account cloud-radiation interactions in considerable detail. This radiation scheme was slightly modified in the longwave radiative transfer calculation to incorporate the Doppler broadening at low pressure, by adding a small constant to the absorber amount, following Fels (1979) and Schwarzkopf and Fels (1991). The longwave cooling rates computed with the original Morcrette (1991) scheme, the modified scheme, and more detailed radiative transfer models that include Doppler broadening, namely a narrow band model (Morcrette et al. 1986) and the GFDL line by line model (Schwarzkopf and Fels, 1991) are shown in Fig.2. When the Doppler broadening is taken into account, the Morcrette scheme gives cooling rates in agreement with that from both the narrow band and the line by line models. The general circulation model - radiation scheme interface was also slightly modified. Between full radiation time steps (the time interval during which the radiative transfer calculation is not updated) a constant net longwave radiative flux is now assumed instead of the original constant effective emissivity. This change was motivated by a numerical instability arising at low pressure when the constant effective emissivity method was used. The source of this instability was traced down to be directly connected to the computation done between full radiation time steps by successfully integrating the GCM with the radiative transfer calculation updated every time step.

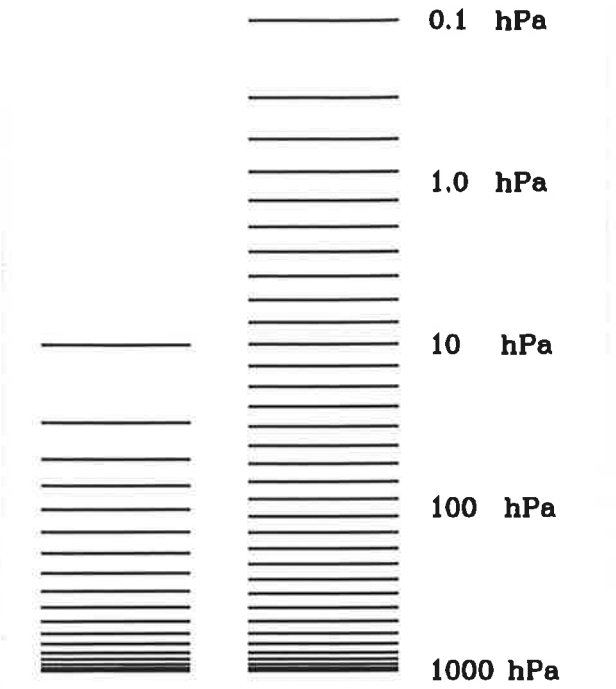

Figure 1 Schematic representation of the pressure levels for the ECHAM3 (19 vertical levels) and ECHAM3.5 (35 vertical levels) models.

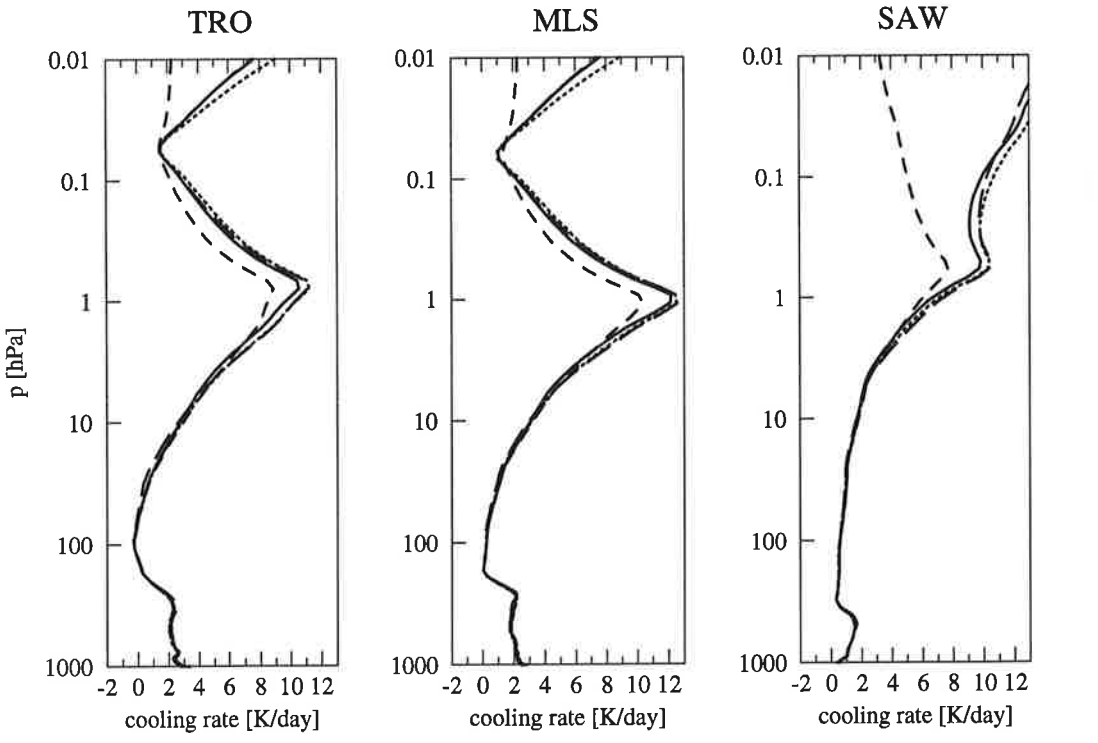

Figure 2 Longwave radiative cooling rates computed from the Morctrette parametrization (dashed); the modified Morctrette parametrization (long dashed); the Morctrette narrow band model (short dashed); and the GFDL line by line model (solid). Column integrations for Tropical (TRO), Mid-Latitude-Summer (MLS), and Sub-Arctic-Winter (SAW) atmospheres (Courtesy of M. Giorgetta).

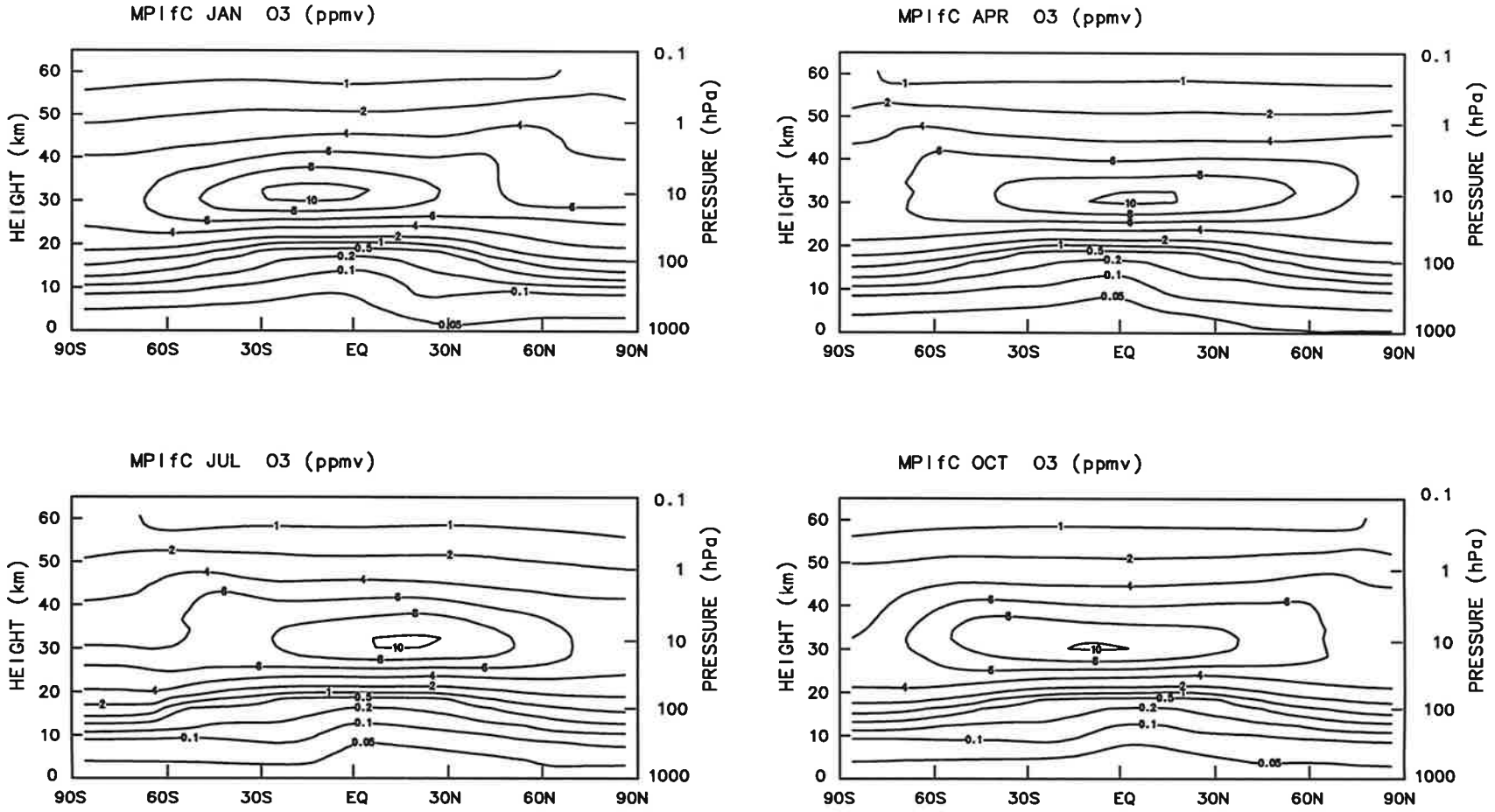

Figure 3 Meridional cross sections of the monthly mean, zonal mean ozone distribution (Brühl, 1993) for January (upper left), April (upper right), July (lower left) and October (lower right). Contours: 0.05, 0.1, 0.2, 0.5, 1, 2, 4, 6, 8, 10 ppmv.

(iv) A prescribed ozone field given by the monthly mean, zonal mean distribution computed with a chemical model (Brühl, 1993) and available from the surface to 0.1 hPa. Meridional cross sections of the ozone distribution for January, April, July and October are shown in Fig.3.

(v) A $2d\nabla^4$ linear horizontal diffusion operator applied to divergence, vorticity, and temperature, with a slightly larger damping time for the latter two fields.

(vi) A three-layer Rayleigh friction applied to vorticity and divergence at the top of the model. This upper-layer damping reduces spurious reflection from upward propagating waves and crudely represents the impact of unresolved mesospheric gravity waves. The damping coefficients from the top are: $(1d)^{-1}$, $(4d)^{-1}$, $(16d)^{-1}$. The damping coefficients are set to zero for the global mean (0,0), and the large scale waves (0,1) and (1,1), as is done for the horizontal diffusion.

In the 20-year simulation performed with the ECHAM3.5 model a T21 horizontal truncation was used. The seasonal cycle in solar radiation was included and climatological monthly mean sea surface temperatures, computed from the so called AMIP 1979-1988 data set (Gates, 1992), were employed. The ozone distribution also varied on a monthly basis as a results of the seasonal cycle included in the chemical model. The diurnal cycle was excluded from the simulation, thus allowing to update the radiative transfer computation every 6 hours. The solar constant and the CO_2 concentration were fixed to present day values. Prior to the 20-year simulation, a total of 14 months were additionally integrated, to allow for spinup. The initial conditions were obtained by a previous integration performed with a slightly different version of the ECHAM3.5 model. Note that the present integration was performed without any orographic gravity wave drag parametrization.

Given that the global observations available reach only 1 hPa (see Section 3) and that the ECHAM3.5 model dynamics can be affected by the upper layer damping above 1 hPa (see Fig.1), results in the following sections will only be presented up to 1 hPa.

3. The dataset of global observations

The dataset of global observations used in the present work was compiled by Randel (1992) from daily geopotential height analyses and consisted of a 12-year climatology (1979-1990) of the troposphere and stratosphere. The daily analyses in the troposphere were originally produced by the National Meteorological Center (NMC) from their operational system at pressure levels 1000, 850, 700, 500, 400, 300, 250, 200, 150, and 100 hPa. In the stratosphere, at pressure levels 70, 50, 30, 10, 5, 2 and 1 hPa, the daily analysis were derived from radiosonde and satellite observations by the Climate Analysis Center (CAC), a department of NMC. For further description of the data see

Randel (1992).

Monthly means of geopotential height fields were kindly provided by W.J. Randel. The dataset consisted of Fourier coefficients up to zonal wavenumber six on a 40-point Gaussian grid (R15) in latitude at the 17 vertical pressure levels specified above.

Shorter records of this dataset have been widely used in previous investigations of the stratospheric climate and variability, see for instance Geller et al. (1983, 1984), Mechoso et al. (1985), Boville and Randel (1986) and Hamilton (1994).

4. Midlatitude tropospheric circulation

The modifications reported in section 2 between the ECHAM3.5 and ECHAM3 models do not appear to dramatically alter the midlatitude large scale tropospheric circulation in the T21 version of the GCMs. This can be seen in Fig.4, where the climatological surface pressure for the December - February (DJF) season from the 20-year simulation with the ECHAM3.5 model is shown. Similarly to the ECHAM3-T21 simulation, the Icelandic low pressure center is of reasonable magnitude but somewhat shifted and confined south-westward. The behavior of the Icelandic low is known to improve at higher horizontal resolution (Boville, 1991; Roeckner et al. 1992; Deque et al. 1994). The Aleutian low in ECHAM3.5 is slightly shallower than in ECHAM3, thus bringing the modified model closer to ECMWF analysis results (see Roeckner et al. 1992 for the ECHAM3 model and ECMWF analysis results).

The simulated 500 hPa 20-year DJF climatology is shown in Fig.5, at left. The East Asia trough is of realistic magnitude, but the American ridge is barely visible. In the Atlantic sector, the East American trough is too weak. These aspects of the simulation are know to improve at higher horizontal resolution and/or using high-order linear horizontal diffusion operators. A discussion of the effects of horizontal diffusion on the large scale circulation can be found in Laursen and Eliasen (1989).

The interannual seasonal variability of the 500 hPa for the DJF season is shown in Fig.5, at right. The amount of variability seen in Fig.5 is comparable to that of a 30-year ECHAM3-T21 simulations with climatological forcing, although its geographical distribution is slightly different in the two GCMs. In both GCMs the seasonal interannual variability is about 70% or more of that computed from ECMWF analyses in the mid-high latitudes (Arpe 1994, personal communication). The mid-high latitude low frequency variability is indeed generally captured also in other low resolution GCMs with climatological sea surface temperature, see for instance Lau and Nath (1987).

The deficiencies in the simulation shown by Fig.4 and Fig.5 can affect the stratospheric

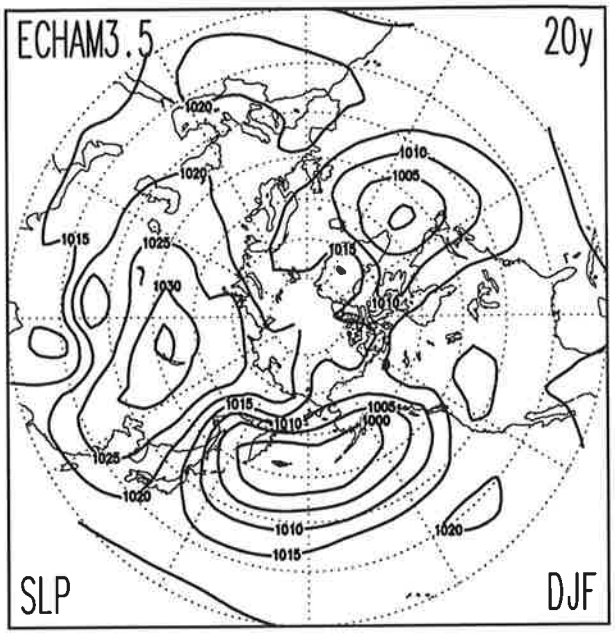

Figure 4 Northern Hemisphere DJF time average surface pressure from the 20-year ECHAM3.5 simulation. Contour: 5 hPa. The outer latitude cycle in this plot and in the following polar stereographic maps is 20°N.

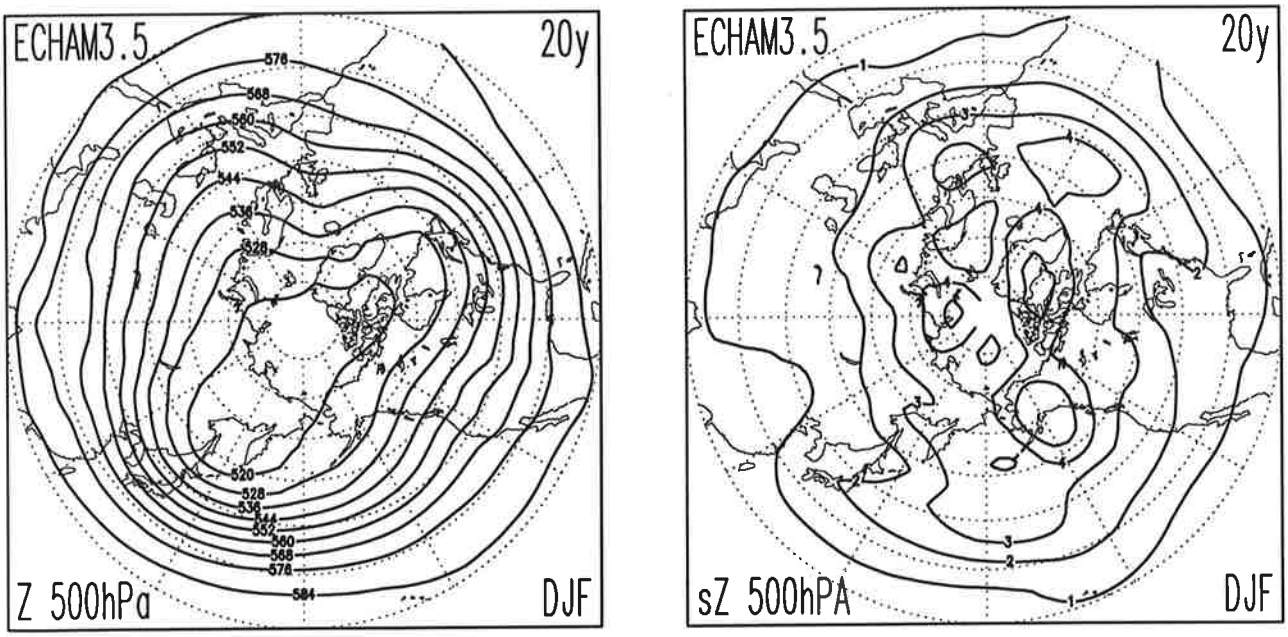

Figure 5 Northern Hemisphere DJF time average 500 hPa geopotential height from the 20-year ECHAM3.5 simulation (contour: 8 dam) at left. Northern Hemisphere DJF interannual variability (standard deviation from the DJF 20-year average, contour: 1 dam) at right.

circulation by altering the tropospheric mechanisms forcing vertically propagating planetary waves. The purpose of this work is therefore limited to evaluate the first order characteristics of the large scale, long term time average state of the stratosphere and its interannual variability.

5. Zonal Mean Circulation

In this section the behavior of the general circulation is presented by meridional cross sections of the zonal mean temperature and zonal wind. The seasonal climate is summarized by considering the December, January and February average (DJF). The interannual variability in the stratosphere is know to show large intraseasonal variations and to generally increases from early to late winter. In the Northern Hemisphere the interannual variability is usually largest in February and March, during the polar vortex breakdown (see for instance Naujokat et al., 1988). The meridional cross sections of the interannual variability (standard deviation) are therefore calculated and presented on a monthly basis.

Fig.6 shows the zonal mean temperature for the DJF time average, from the NMC-CAC observations and the ECHAM3.5 simulation. The NMC-CAC climatology is a 12-year average (1979-1990), while the ECHAM3.5 climatology is a 20-year average. Averages from the simulation on a time scale comparable to the length of the analyses record, i.e. 10 years, give virtually identical fields.

The NMC-CAC observations (Fig.6, upper panel) show that in the troposphere the climatological zonal mean temperature rapidly decreases with height, the coldest temperature (about 200°K) occurring at the equatorial tropopause. In the tropics and in the Southern Hemisphere (SH), the climatological zonal mean temperature increases with height above the tropopause. In the Northern Hemisphere (NH) the climatological zonal mean temperature decreases with height up to the lower stratosphere, where another local minimum of about 210°K is found. At the stratopause the zonal mean temperature is largest at the South Pole (about 280°K).

The general behavior of the simulated DJF time average zonal mean temperature (Fig.6, lower panel) is considerably close to the observed one. In the troposphere the climatological zonal mean temperature rapidly decreases with height and the equatorial tropopause minimum is of realistic magnitude (about 200°K). In the tropical stratosphere and in the Southern Hemisphere stratosphere the climatological zonal mean temperature increases with height in reasonable agreement with observations, although the maximum at the stratopause South Pole is underestimated, not exceeding 270°K. In addition, in the upper troposphere and lower stratosphere of the Northern Hemisphere the minimum is about 5°-10°K colder in the model. A global cold bias of few degrees at the tropopause is also apparent.

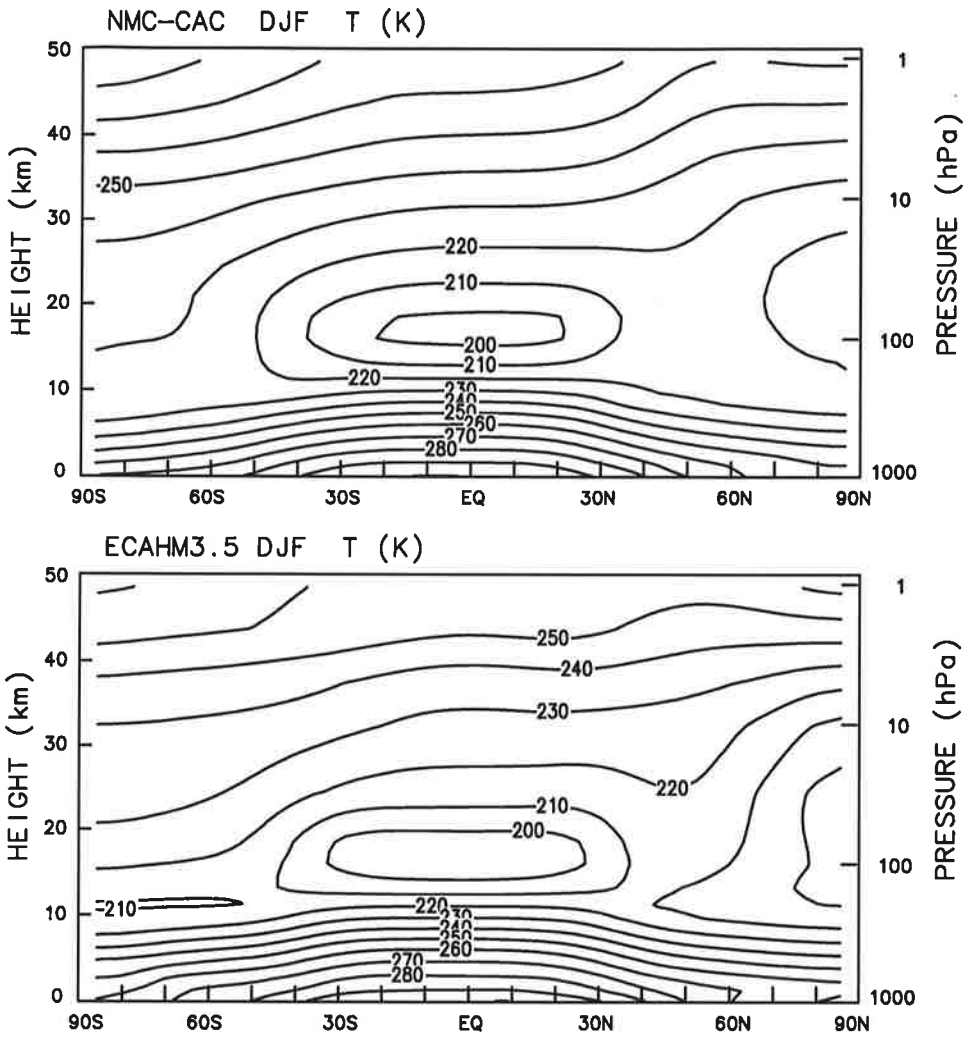

Figure 6 DJF time average zonal mean temperature from the 12-year NMC-CAC observations (upper panel) and from the 20-year ECHAM3.5 simulation (lower panel). Contour: 10^{o} K.

The corresponding DJF time average zonal mean zonal wind is shown in Fig.7. Good features of the simulation include the clear separation between the tropospheric and stratospheric westerly jets in the NH lower stratosphere and the confinement to the troposphere of the subtropical jet in the Southern Hemisphere. In the troposphere, the location of the subtropical jets is well represented in the simulation. The summer jet is however stronger (5-10 ms^{-1} more) than that seen in the NMC-CAC data. In the lower stratosphere, the observed and simulated stratospheric westerly jets are of comparable magnitude and are both strongest around 60°-70°N. In the upper stratosphere the simulated westerly jet is instead too weak equatorward of 50°N and too strong poleward of 60°N. The polar confinement of the simulated westerly jet is a particularly pronounced feature in the December and January climatologies, while it is absent in February. This is shown in the Appendix (Fig.A1 and Fig.A2) where the climatological

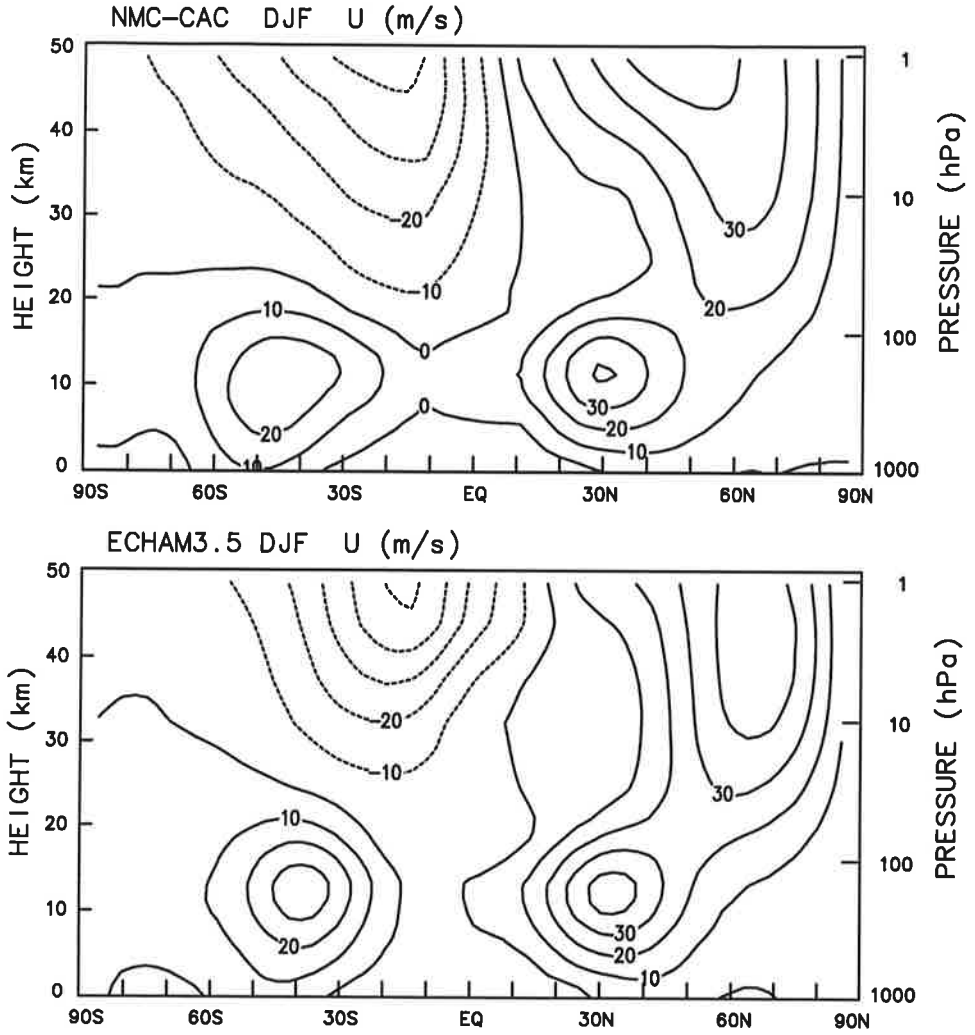

Figure 7 DJF time average zonal mean zonal wind from the 12-year NMC-CAC observations (upper panel) and from the 20-year ECHAM3.5 simulation (lower panel). Contour: 10 ms^{-1}.

monthly mean, zonal mean zonal winds for the three winter months from the NMC-CAC and ECHAM3.5 datasets are respectively shown. Note that Fig.A1 and Fig.A2 also show that the observed abrupt decrease in strength in the stratospheric westerly jet from January to February is well simulated by the ECHAM3.5 model. In the Southern Hemisphere, both the observed and simulated easterly mean winds are weak in the lower stratosphere. In addition, the observed and simulated easterly mean jets have comparable magnitudes and peak between 10°S and 30°S.

The most likely cause of the polar confinement of the winter stratospheric jet and of the cold polar bias in the lower stratosphere is an improper treatment of both resolved and unresolved gravity waves in low resolution GCMs. The cold bias at the South Pole stratopause (Fig.6) may instead be related to the location of the model top in the middle

mesosphere (0.1 hPa, that might be too low) and/or to unrealistic effects of the mesospheric drag on the mean meridional circulation (that might be too strong).

The interannual variability (standard deviation) of the monthly mean, zonal mean temperature from the NMC-CAC 12-year average is shown for December, January and February in Fig.8. Most of the variability in the Northern Hemisphere arises from interannual variations in the large scale stratospheric circulation. The stratospheric extra-tropical circulation is known to be strongly affected by vertically propagating planetary waves (Charney and Drazin, 1961). Episodes of anomalously large planetary waves can substantially displace the westerly vortex and therefore cause sudden warmings of the stratosphere in the polar region (Matsuno, 1971; Labitzke, 1981). In the Southern Hemisphere and in the tropics, causes associated with direct external forcing should be responsible of most of the variability seen in Fig.8, although spurious variability (of the order of few degrees) due to changes in data acquisition also contribute in the upper stratosphere, above 10 hPa (Randel, 1992; Finger et al., 1993).

In the Northern Hemisphere, the December interannual variability of the zonal mean temperature increases poleward and reaches 6°K in the lower-middle stratosphere (Fig.8, upper panel). The variability seen in December in the Southern Hemisphere is presumably associated with the final stages of the SH polar vortex breakdown. In January (Fig.8, middle panel), the interannual variability is larger than in December throughout the whole stratosphere, poleward of 60°N. The interannual variability in the NH high latitudes also increases from January to February, especially in the upper stratosphere. The increase in interannual variability from December to January and February seen in the NMC-CAC data is consistent with the generally observed occurrence of major and/or final sudden stratospheric warming events in late winter. This is illustrated for instance by the frequency distribution of the North Pole monthly mean temperature at 30 hPa from NH observations subjectively analyzed at the Free University Berlin, recently updated in Pawson et al. (1993)

Fig.9 shows the interannual variability of the monthly mean, zonal mean temperature from the 20-year ECHAM3.5 simulation. Fig.9 indicates that a considerable amount of variability is present in the simulation during the NH winter season and that the simulated variability increases from December to January and February, in broad agreement with observations (Fig.8). Moreover, the simulated variability is also negligible in the tropics and in the Southern Hemisphere (except close to the South Pole in December, lower stratosphere), supporting the external and/or spurious origin of the variability outside the Northern Hemisphere in the NMC-CAC data. The few degree of variability in December near the South Pole must be associated with the late breakdown of the Southern Hemisphere polar vortex. Although the simulated standard deviation in zonal mean temperature increases poleward as in the observations, its vertical structure somewhat disagrees with that shown in Fig.8. Firstly, in the upper troposphere and lower stratosphere the December interannual variability is substantially underestimated in the

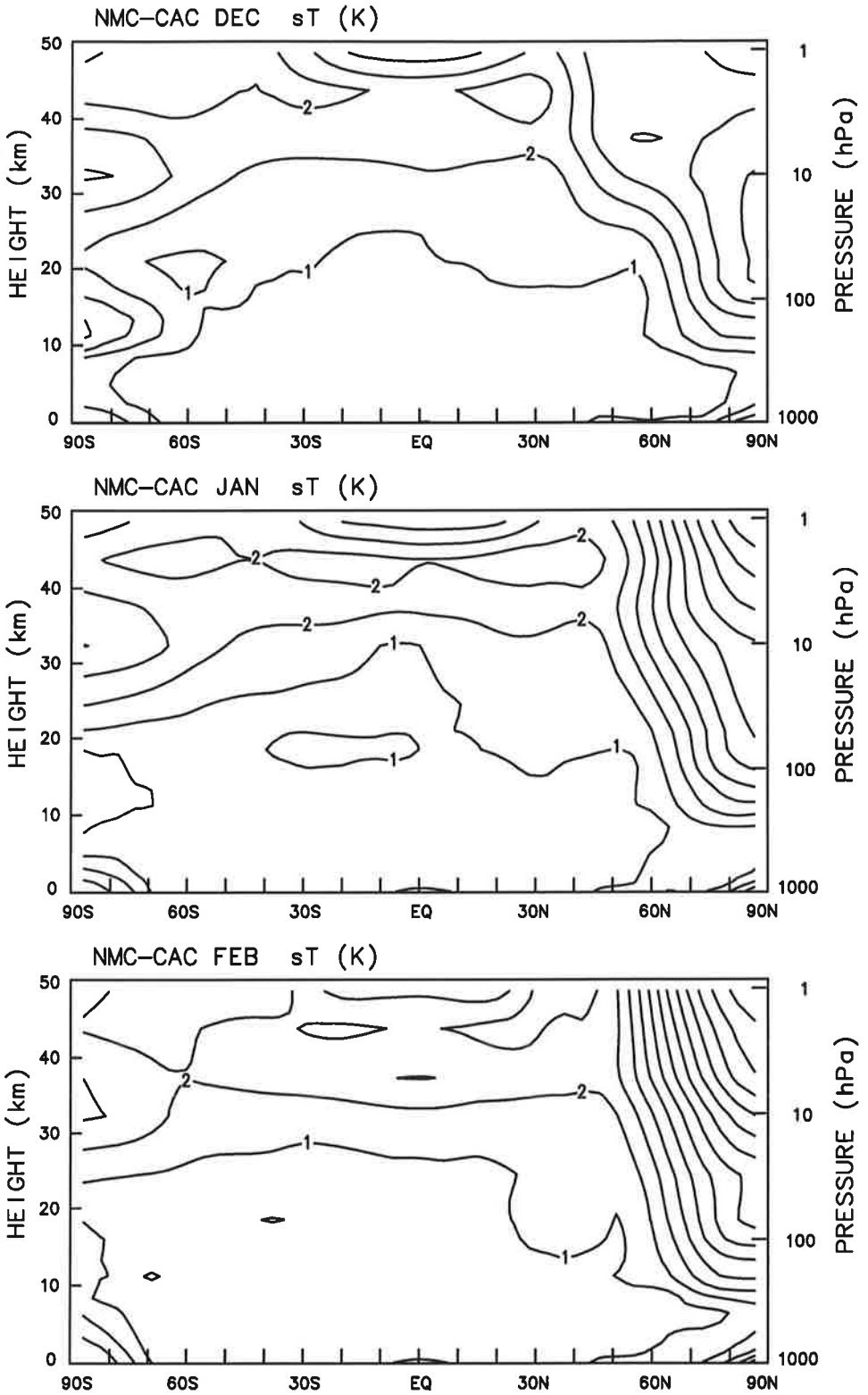

Figure 8 Monthly interannual variability (standard deviation) of the zonal mean temperature from the 12-year NMC-CAC observations for December (upper panel), January (middle panel), and February (lower panel). Contour: 1^{o} K.

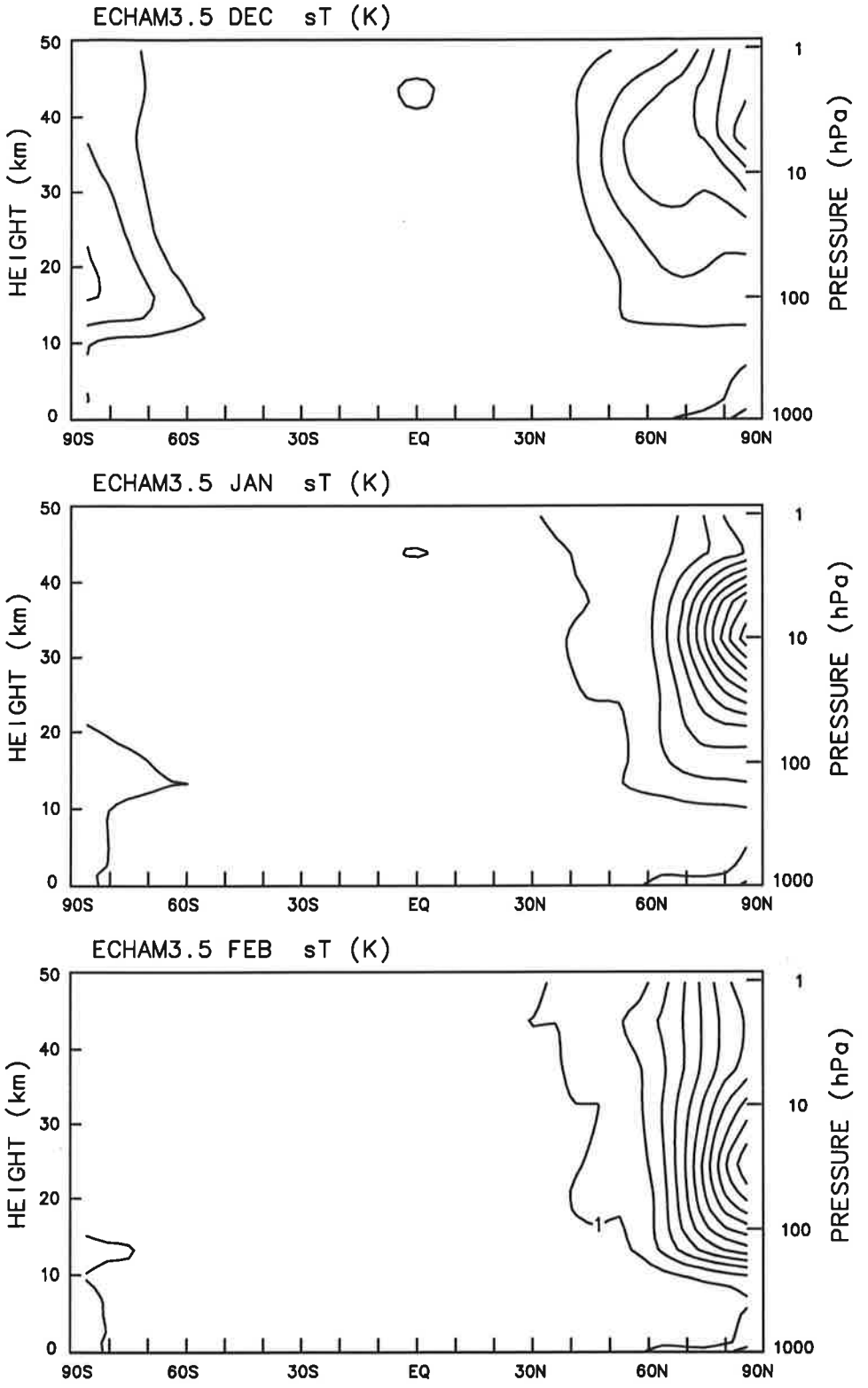

Figure 9 Monthly interannual variability (standard deviation) of the zonal mean temperature from the 20-year ECHAM3.5 simulation for December (upper panel), January (middle panel), and February (lower panel). Contour: 1^{o} K.

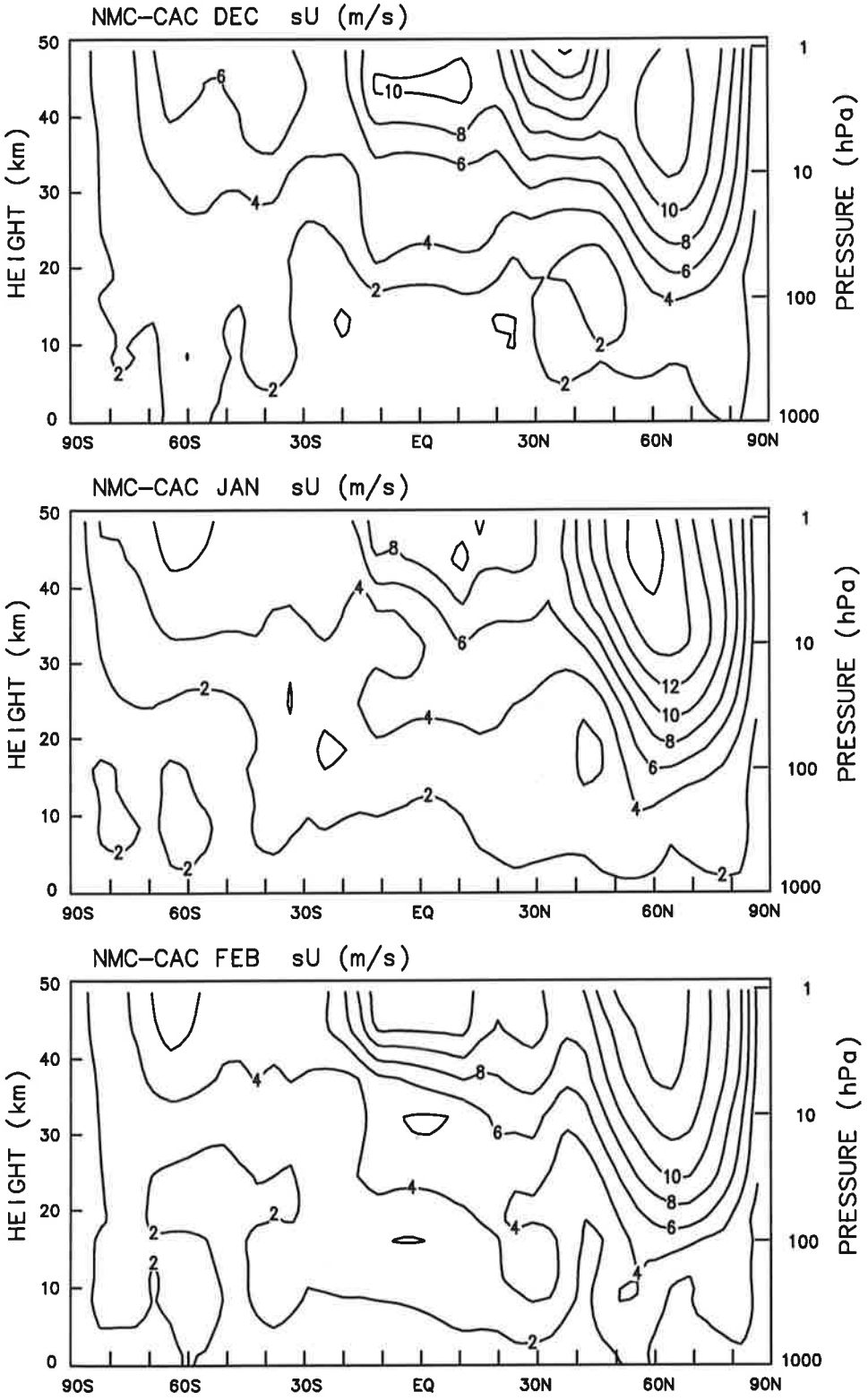

Figure 10 Monthly interannual variability (standard deviation) of the zonal mean zonal wind from the 12-year NMC-CAC observations for December (upper panel), January (middle panel), and February (lower panel). Contour: 2 ms^{-1}.

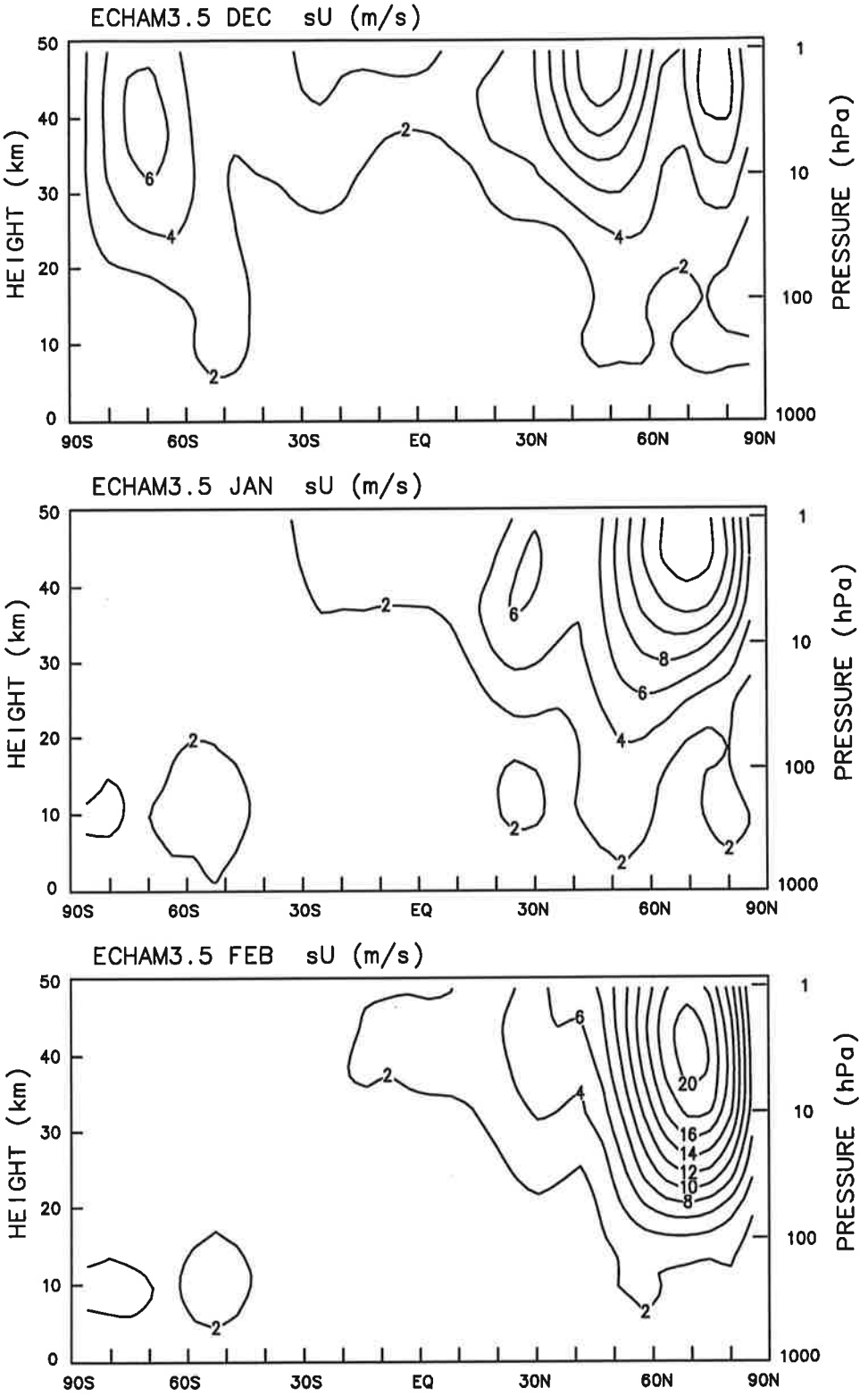

Figure 11 Monthly interannual variability (standard deviation) of the zonal mean zonal wind from the 20-year ECHAM3.5 simulation for December (upper panel), January (middle panel), and February (lower panel). Contour: 2 ms^{-1}.

GCM. Secondly, in January and February the simulated variability is largest in the middle and lower stratosphere. Note however that the NMC-CAC variability in the zonal mean temperature in the upper stratosphere can be actually overestimated (Finger et al., 1993). The December underestimation may be caused by insufficient horizontal resolution in the troposphere, hence leading to a weak dynamical forcing of the stratosphere. The behavior in the middle stratosphere may be related to an excessively large temperature gradient over the North Pole at 10 hPa (see section 5 and Fig.A3, upper panel) that could spuriously amplify variations in the monthly mean temperature.

The monthly interannual variability of the zonal mean zonal wind from the 12- year NMC-CAC observations is presented in Fig.10. The corresponding simulated fields for the 20-year ECHAM3.5 simulation are shown in Fig.11.

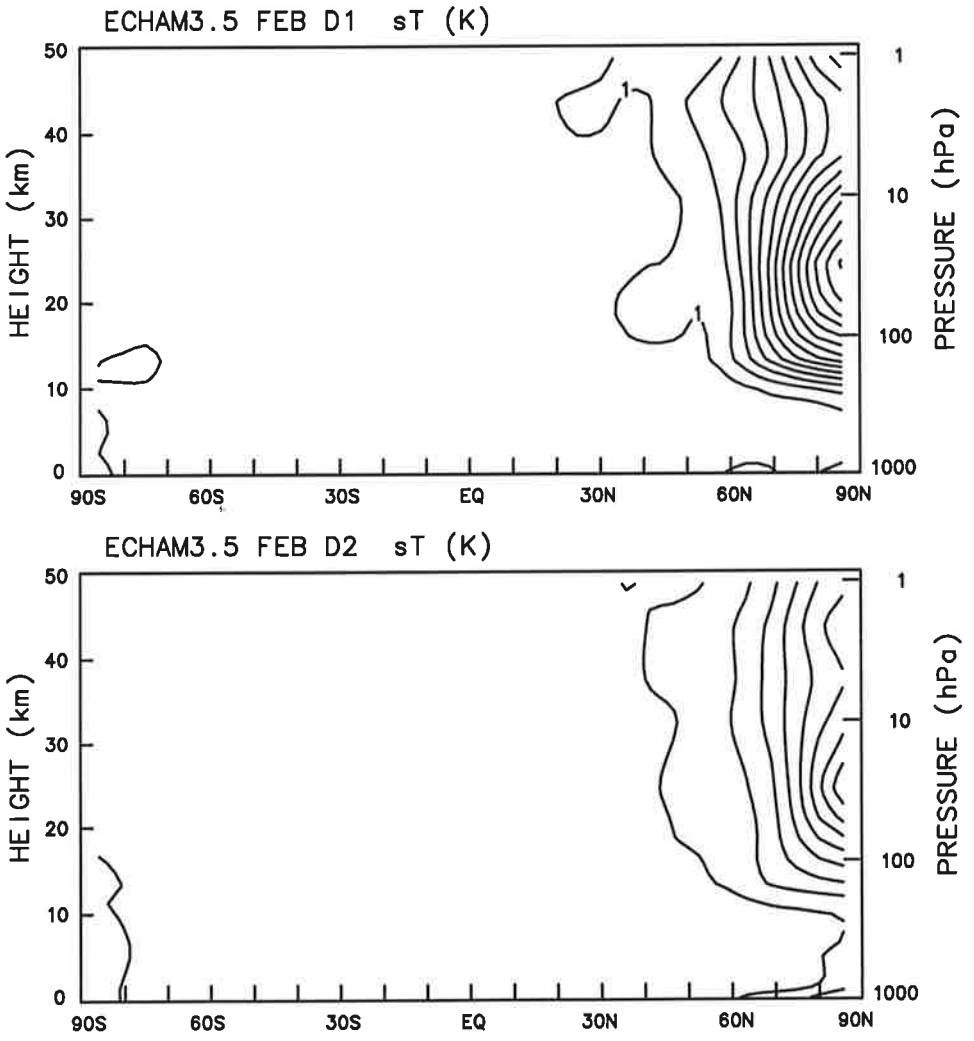

Figure 12 February interannual variability (standard deviation) of the zonal mean temperature from the first decade of the ECHAM3.5 simulation (upper panel) and from the second decade of the ECHAM3.5 simulation (lower panel). Contour: 1^{o} K.

The December NMC-CAC interannual variability zonal mean zonal wind is characterized by two large maxima in the NH stratosphere, and a third weaker maximum at the equatorial stratopause (Fig.10, upper panel). The NH variability peaks should be associated with displacements of the polar westerly vortex, while the equatorial variability might be connected to variations in the semi-annual oscillation in zonal wind at the equatorial stratopause. The largest variability in the zonal mean zonal wind is located between 30°N and 40°N in the upper stratosphere. The second variability maximum is located between 60°N and 70°N and extends throughout most of the stratosphere. In December, the simulated interannual variability in zonal mean zonal wind (Fig.11, upper panel) is characterized by a pattern similar to that observed. However, both the NH variability maxima are shifted northward by about 10° of latitude in the model and the maximum at high latitudes is not sufficiently developed in the lower

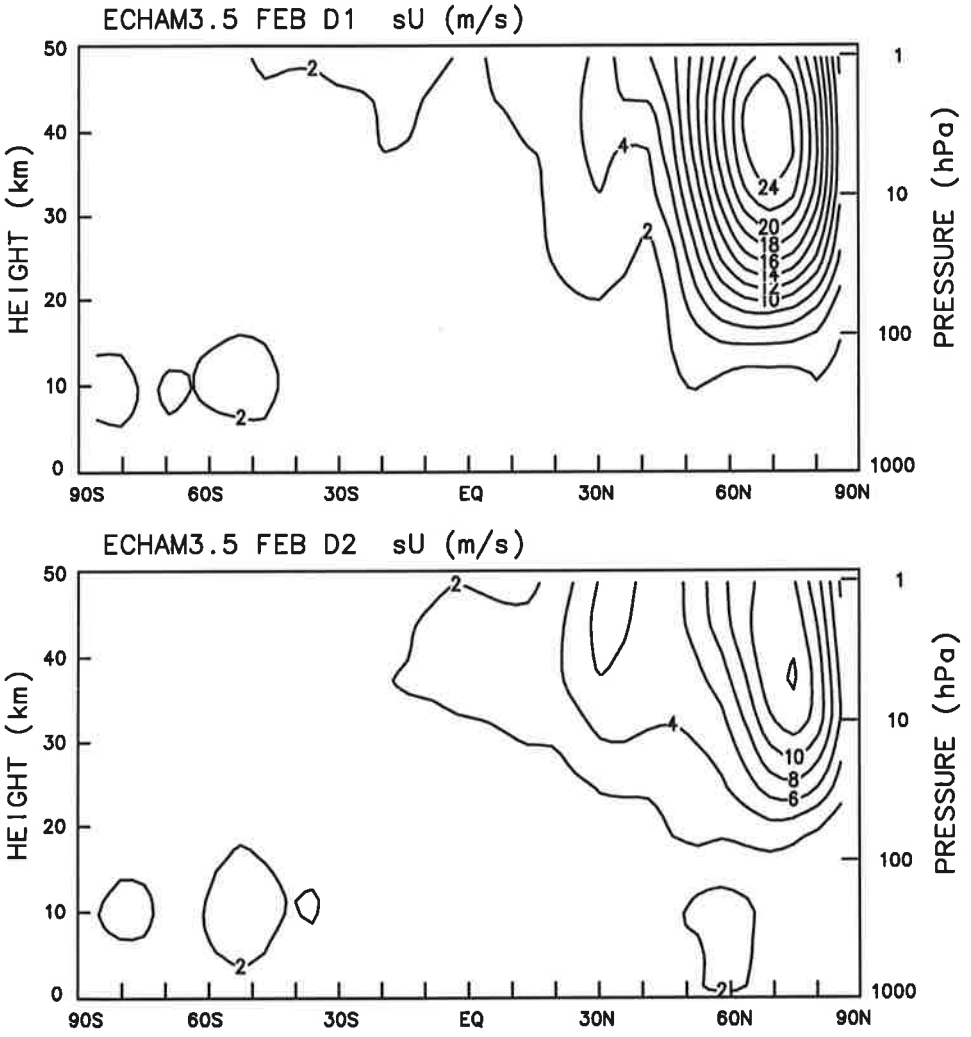

Figure 13 February interannual variability (standard deviation) of the zonal mean zonal wind from the first decade of the ECHAM3.5 simulation (upper panel) and from the second decade of the ECHAM3.5 simulation (lower panel). Contour: 2 ms^{-1}.

stratosphere. The January interannual variability of the zonal mean zonal wind from both the NMC-CAC data (Fig.10, middle panel) and the simulation (Fig.11, middle panel) show one major peak, located poleward of 30°N. Also during January the variability is somewhat underestimated in the lower stratosphere in the model. A change in the behavior of the simulation appears to occur in February, when the simulated stratosphere (Fig.11, lower panel) clearly show a high level of interannual variability at middle and high latitudes, quite comparable to the observed one (Fig.10, lower panel). The region of enhanced variability is shifted poleward in the simulation also in January and February. This poleward shift with respect to observations may be associated with the poleward confinement of the simulated climatological stratospheric westerly jet (see Fig.7).

Contrary to the behavior of the climatological averages, in February the simulated monthly interannual variability computed from a 10-year sample can be quite different from that shown in Fig.9 and Fig.11, computed from the full 20-year sample available from the integration. This is illustrated in Fig.12 and Fig.13, where the February interannual standard deviation is separately computed from the first and from the second decade of the 20-year simulation. Fig.12 and Fig. 13 respectively shows the interannual variability of the zonal mean temperature and zonal wind. Clearly, during the second decade the February interannual variability is about half that of the first decade. The cause of this apparently low-frequency variation during February is further analyzed in the next section. In January and December, on the other hand, the two decadal integrations are characterized by only slight changes in the monthly interannual variability (not shown).

6. Quasi-stationary planetary waves

Polar stereographic maps at selected pressure levels are presented, in order to evaluate the simulated quasi-stationary planetary waves against the NMC-CAC observations. Long term averages and monthly interannual standard deviations were calculate from monthly mean geopotential height and temperature fields. In the following, the results obtained from the monthly mean temperatures are shown.

The Northern Hemisphere DJF time average temperature at 50 hPa from the 12-year NMC-CAC observations and the 20-year ECHAM3.5 simulation is shown in Fig.14. The simulated DJF climatological temperature clearly captures the stationary wave pattern seen in the NMC-CAC data. Both the observed and simulated climatological temperatures are characterized by warm air over the North-Western Pacific Ocean and cold air north of Scandinavia. Fig.14 also show that the magnitude of the model's polar cold bias is within about 5°K in the lower stratosphere.

The DJF time average temperature in the middle and upper stratosphere (shown in the

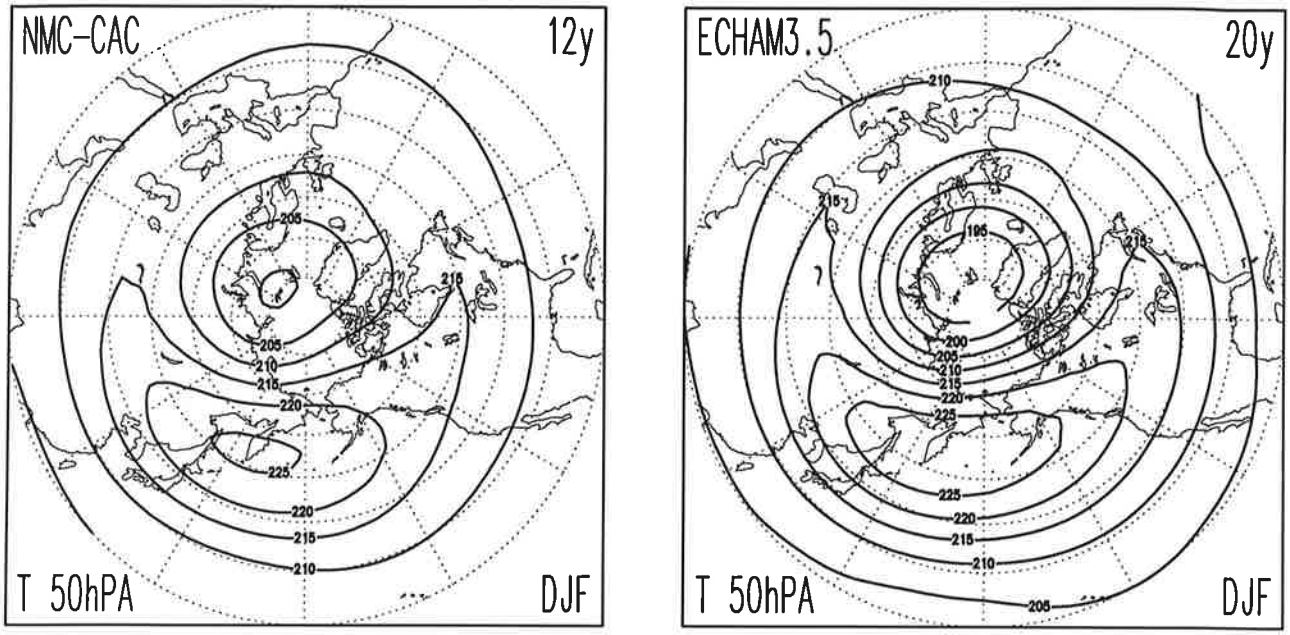

Figure 14 Northern Hemisphere DJF time average temperature at 50 hPa from the 12-year NMC-CAC observations (at left) and from the 20-year ECHAM3.5 simulation (at right). Contour: 5° K.

Appendix, Fig.A3) indicate that the simulation captures the structure and the westward phase tilt with height of the observed quasi- stationary planetary waves. However, the amplitude of the simulated planetary waves seems to be generally overestimated in the middle and upper stratosphere. In addition, the model's cold polar bias is worse at 10 hPa than in the lower stratosphere (at 50 hPa, Fig.14) and over the North Pole the simulated climatological temperature gradient is too large. The model's cold polar bias is virtually disappeared at 1 hPa.

The interannual variability of the monthly mean temperature for December, January and February at 50 hPa from the NMC-CAC observations and ECHAM3.5 simulation are shown in Fig.15.

In December the observed variability (Fig.15a) has a roughly zonally symmetric pattern, increasing poleward from about 3°-4°K at 60°N to 6°K at the North Pole. The inspection of the individual NMC-CAC monthly mean temperatures for the 1979-1990 period suggests that the planetary wavenumber one is a dominant feature of the circulation in December, although its pattern may be modulated by amplifications/reductions of the Aleutian high. An exception is December 1987, when the cold air center north of Scandinavia virtually disappeared. In December 1987 an unusually early winter major warming was indeed reported also from other observations (Naujokat et al., 1988).

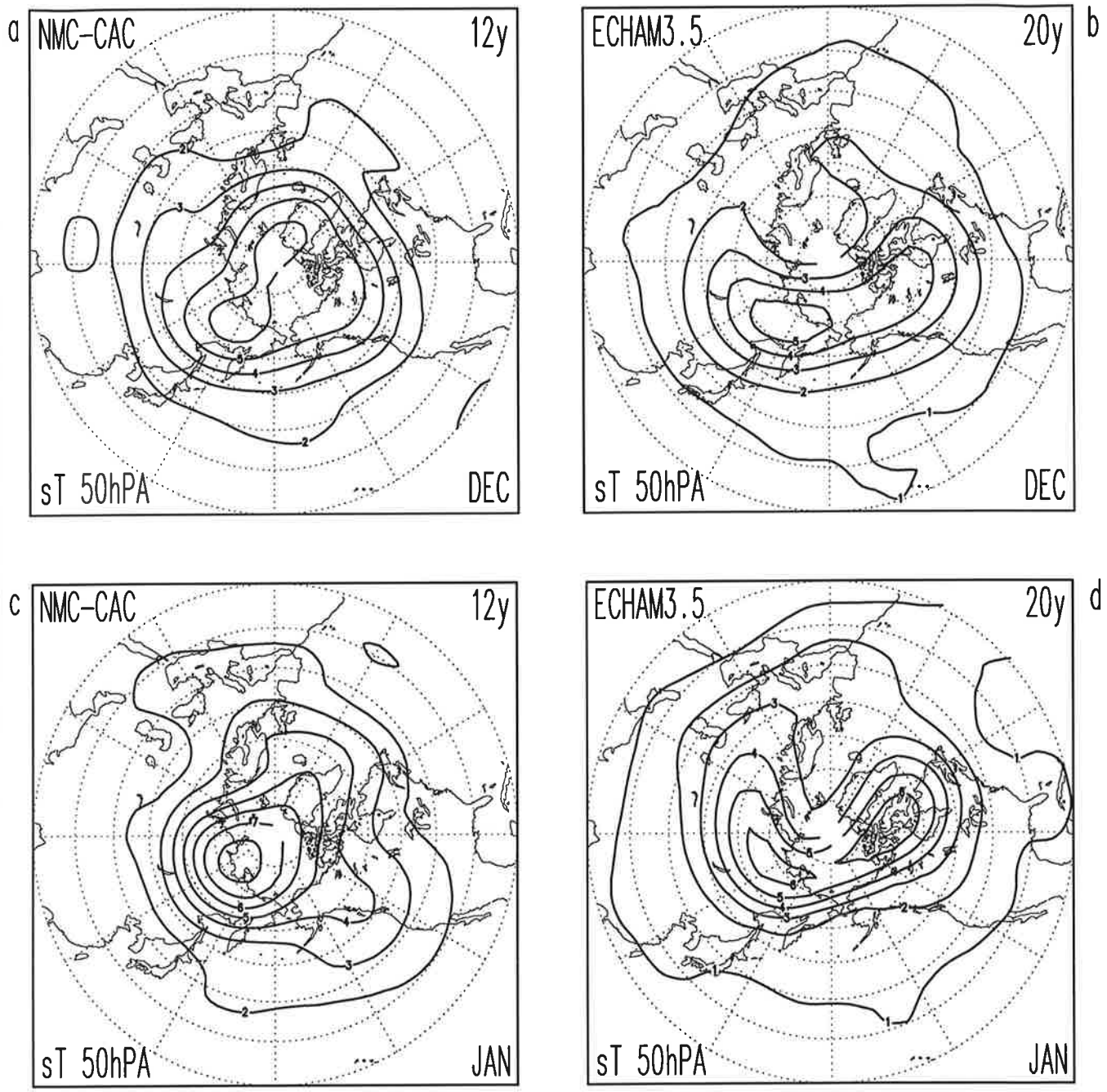

Figure 15 Northern Hemisphere monthly interannual variability (standard deviation) temperature at 50 hPa from the 12-year NMC-CAC observations (left column) and from the 20-year ECHAM3.5 simulation (right column) for (a) and (b) December; (c) and (d) January; (e) and (f) February. Contour: 1^{o} K.

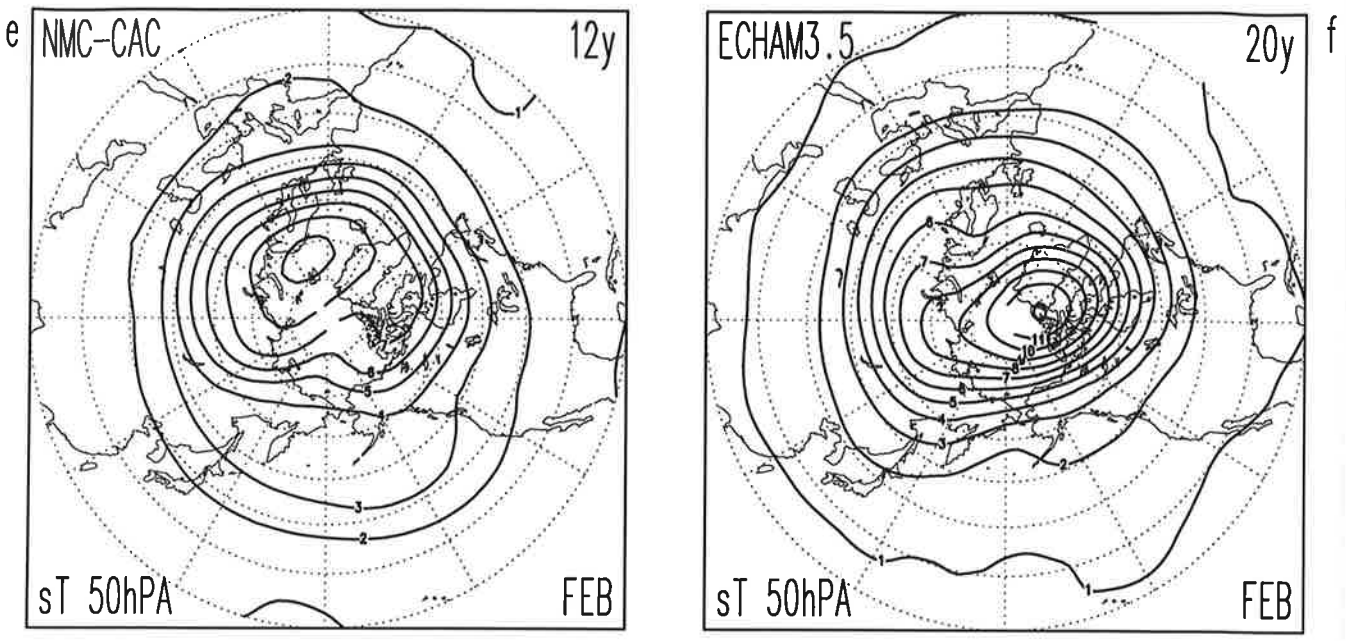

Figure 15 (continued).

The December simulated variability (Fig.15b) is comparable to that observed over Northern Canada and North-East Asia, where it reaches 5°K. North of Scandinavia the monthly interannual variability is instead quite low in the GCM, barely exceeding 1°K. The individual monthly mean temperatures from the 20-year simulation indicate that in the model the cold air center is locked to the December climatological position and magnitude (similar to that shown in Fig.14). This behavior therefore explains the lack of variability north of Scandinavia seen in Fig.15b, and suggests that the model cold bias and the variability low might be strongly interdependent. Moreover, the persistent dominance of planetary wavenumber one in the 20 simulated Decembers appears to impede the occurrence of any warming event so strong and long enough to be visible in a monthly mean, as in the case of December 1987. The major cause of interannual variability in the model appears to be the stretching of the North-Western Pacific warm air center toward Asia or alternatively North America. This is actually a realistic feature, characterizing most of the NMC-CAC interannual variability. The simulated interannual variability of the monthly mean geopotential height (not shown) was also found to be comparable to that observed in proximity to the Aleutian high and severely underestimated north of Scandinavia, consistently with the monthly mean temperature variability pattern. In the middle and upper stratosphere the simulated interannual variability behaves in a similar way, with localized regions of enhanced and/or reduced variability (not shown).

The observed January interannual variability peaks over North-Eastern Asia, at about 7°K, see Fig.15c. The individual NMC-CAC monthly mean temperatures show that also during January the planetary wavenumber one pattern is a rather stable feature in the lower stratosphere. During 1979-1990 the wavenumber one is indeed clearly present in every year except in January 1985, when a major mid-winter warming occurred (see also Naujokat et al. 1988). Fig.15d shows that the simulated January interannual variability is comparable in magnitude to that observed over North America and over North-Eastern Asia, reaching at 6°K. Fig.15d also shows that the variability low characterizing the North-Western Atlantic region in December is only slightly alleviated in January. Monthly mean temperatures from individual model year indicate that the lower stratospheric circulation is dominated by a persistent planetary wavenumber one pattern, as in the observations. Similarly to the December monthly mean temperatures, most of the simulated variability appears to be caused by warm air tongues wrapping around the cold air center. This behavior is in qualitative agreement with that of the NMC-CAC monthly mean temperatures. However, in the simulation the cold core of the polar vortex appears to be overly static and deep, similarly to the December case. Again, no monthly mean warming like January 1985 were found in the individual monthly mean temperatures from the 20 simulated Januaries. The main reason to this is presumably the low horizontal resolution used in the simulation.

The NMC-CAC interannual variability continues to increase in the middle and upper stratosphere, while in the simulation the variability starts to decrease in the upper stratosphere. Given the uncertainty in both observations (change in data acquisition, Finger et al. 1992) and simulated data (proximity of the upper-layer damping), the upper stratosphere is not analyzed in detail in this work.

In February (Fig.15e) the observed interannual variability over Europe and the North Atlantic Ocean is about 30% larger than that of the two previous months, ranging from 5°K-6°K at 60°N to 9°K north of Scandinavia. The increase in variability in late winter was already noted in the meridional cross sections. In the ECHAM3.5 model the rate of increase in variability from December to February is actually even larger, reaching a maximum north of Scandinavia (Fig.15f). The sharp variability minimum seen in December over Europe and the North Atlantic Ocean virtually disappeared in February, when the simulated interannual variability compare well with that observed. The location and intensity of the variability maximum are somewhat different in the ECHAM3.5 and NMC-CAC data. However, the characteristic variability maximum is very much influenced by a few extreme months, suggesting that a dataset longer than 12 years would be necessary to settle the variability distribution. The February interannual variability at 50 hPa based on a 28 year record (Free University Berlin, see Pawson et al. 1993) shows indeed a slightly more zonally symmetric pattern.

The interannual standard deviation of the February mean temperature at 10 hPa is shown in Fig.16. Note that the simulated variability is computed from the 20-year record (upper

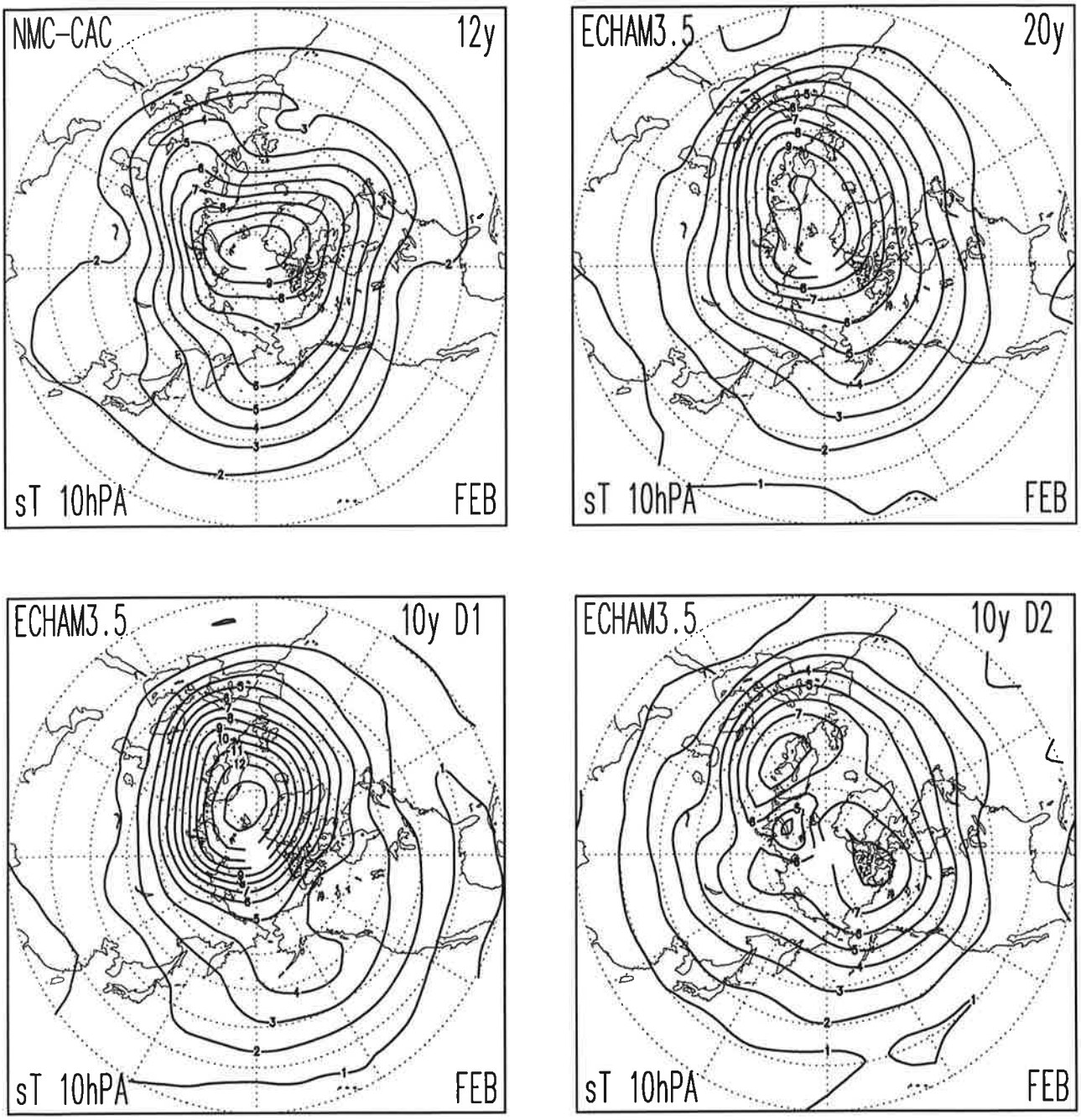

Figure 16 Northern Hemisphere February interannual variability (standard deviation) temperature at 10 hPa from the 12-year NMC-CAC observations (upper left); from the 20-year ECHAM3.5 simulation (upper right); from the first decade of the ECHAM3.5 simulation (lower left); and from the second decade of the ECHAM3.5 simulation (lower right). Contour: 1^{o} K.

panel, on the right) as well as from the first and second decades separately (lower panels). Consistently with the meridional cross sections of the February interannual variability of the zonal mean temperature, the polar stereographic maps show that the interannual variability of the February temperature at 10 hPa is larger than that at 50 hPa, both in the observations and in the model. The interannual variability computed from the 20-year record compare well with that derived from the NMC-CAC analyses, both in magnitude and in structure.

As expected from the monthly mean, zonal mean results (see Fig.12 and Fig.13), the simulated variability of the February mean temperature at 10 hPa for the first decade is about twice that computed from the second decade (Fig.16, lower panels). In addition, the interannual variability in the first decade is characterized by a single maximum, north of Scandinavia, while two distinct maxima occur in the second decade, one over Northern Europe and the other north of Northern Canada. A similar behavior is obtained for the interannual variability computed from the two decades separately at 50 hPa and from the monthly mean geopotential height field (not shown).

An inspection of the ECHAM3.5 individual February temperatures at 50 hPa shows that on two occasions, namely year 7 and year 10 of the 20-year integration, the simulated monthly mean polar temperatures are much warmer than the climatological average, thus suggesting the occurrence of sudden stratospheric warming type events. The intensity of the two simulated polar warmings are indeed comparable to that observed in

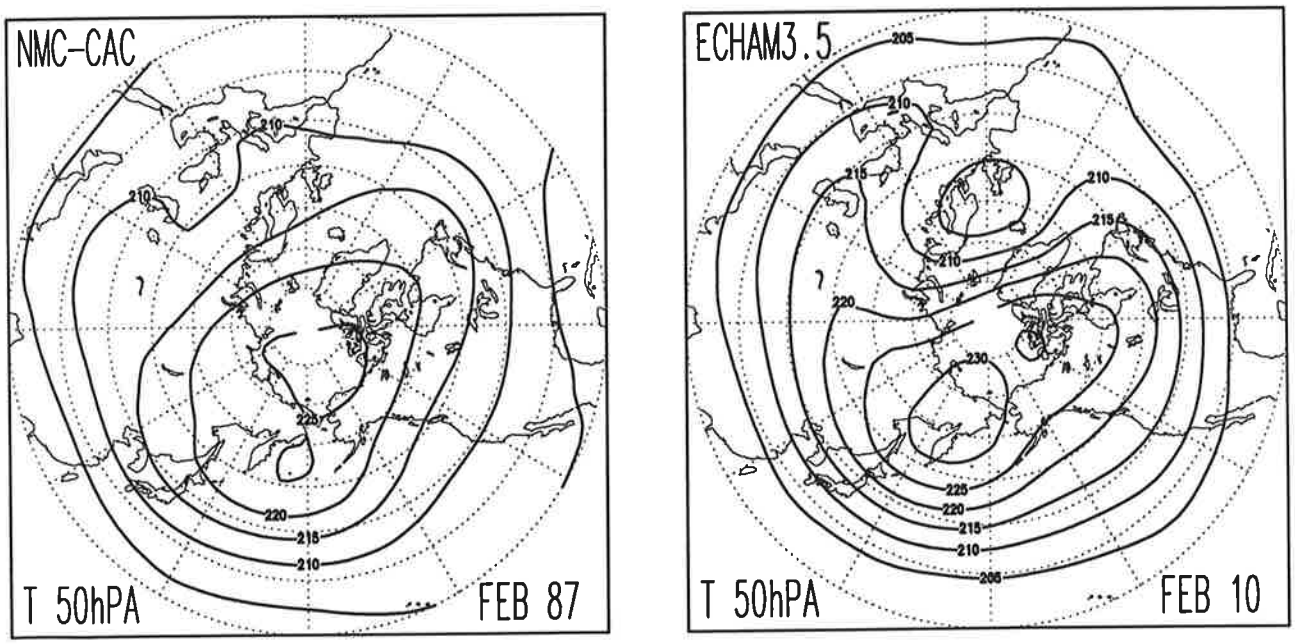

Figure 17 Northern Hemisphere monthly mean temperature at 50 hPa for the NMC-CAC February 1987 at right and for the ECHAM3.5 February year 10 at left. Contour: 5° K.

February 1987, when a major mid-winter warming occurred (Naujokat et al. 1987). This can be seen in Fig.17, where the NMC-CAC February 1987 mean and the ECHAM3.5 February temperature for year 10 at 50 hPa are reported. This result suggests that the reason for the difference in the two 10-year samples during February (Fig.12, Fig.13 and Fig.16, lower panels) is caused by the occurrence of two extreme warmings within the first decade (year 7 and 10), while none of such events were found during the second decade. Note that the North Pole temperature observations reported from Naujokat et al. (1988) for the NH winter from 1966 to 1988 show that an interval of 10 years or more between February major warmings could actually be realistic.

The intensity of the simulated warming can also be seen in Fig.18, where the monthly mean, zonal mean zonal wind for February 10 is show, lower panel. For comparison,

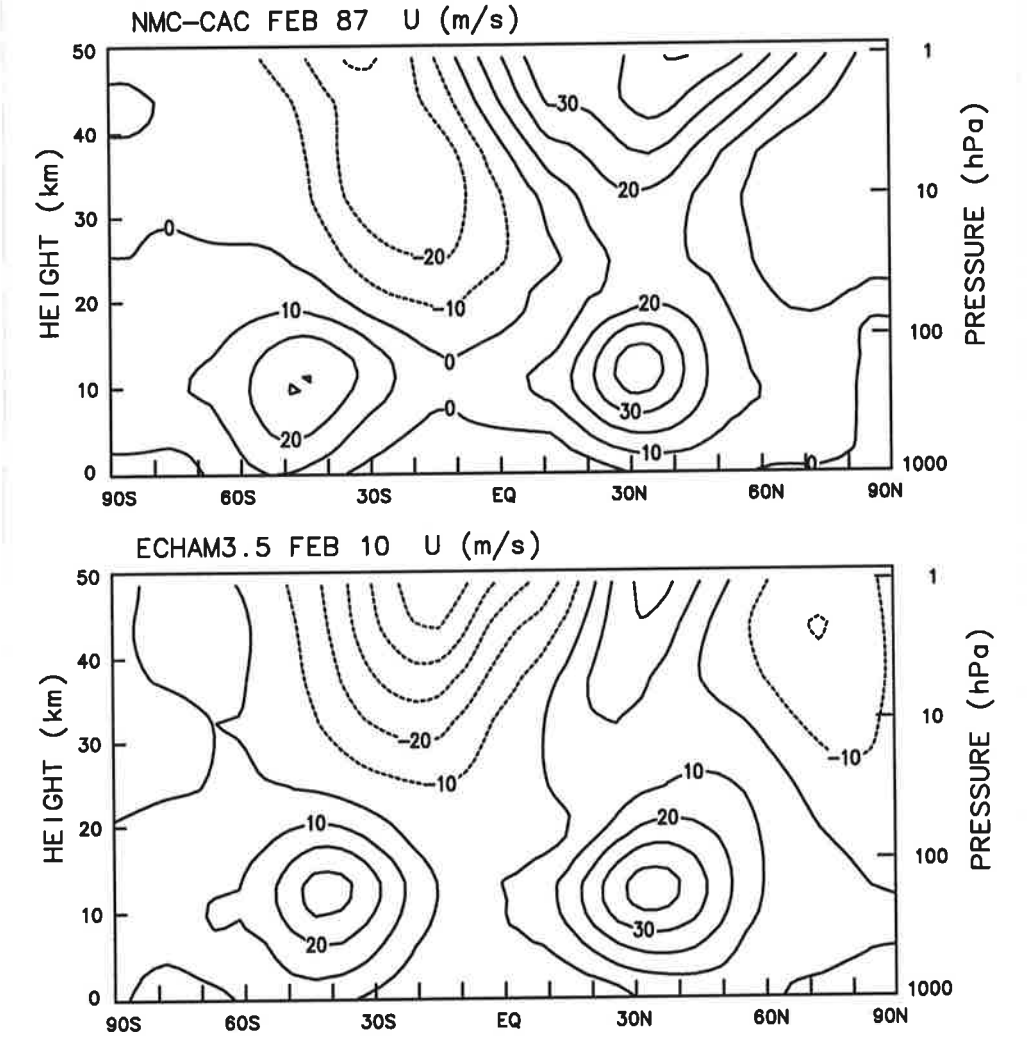

Figure 18 Monthly mean, zonal mean zonal wind for the NMC-CAC February 1987 (upper panel) and for the ECHAM3.5 February year 10 (lower panel). Contour: 10 ms^{-1}.

also the NMC-CAC February 87 zonal mean zonal wind is presented, upper panel. Clearly, in both the observed and simulated Februaries the occurrence of the polar warming was strong enough to reverse the zonal mean circulation poleward of 60°N in the middle stratosphere. This result indicates that a spontaneous major and/or final warming occurred in the simulation. Further detailed analyses of the daily evolution of the simulated warmings are beyond the purpose of this work and will be examined in a following paper.

7. Conclusions

The climate and the natural variability of the stratosphere from a model simulations and from global observations have been examined. The simulation was performed with the newly developed ECHAM3.5 general circulation model, integrated for 20-years, and the global observations were compiled by Randel (1992) from 12-year NMC-CAC operational analyses.

The ECHAM3.5 model is a modified version of the ECHAM3 general circulation model and is part of a general project aimed at developing the cycle-4 of the ECHAM general circulation models. Novel model features with respect to ECHAM3 include a semi-Lagrangian transport of liquid water and water vapor, the Morctrette (1991) radiation scheme, and a prescribed ozone distribution available from the surface to 0.1 hPa. Most importantly, the ECHAM3 vertical structure was extended from 19 to 35 vertical levels and the model top was raised from 10 hPa to 0.1 hPa. In addition, an upper layer damping was included in the mesosphere (i.e., above 1 hPa). In this work the focus was on evaluating the behavior of the ECHAM3.5 general circulation model in the stratosphere in a long-term climate simulation. Therefore a relatively low horizontal resolution was used (T21). The seasonal cycle in solar radiation was included in the simulation and climatological sea surface temperatures were used. The simulation was performed without any gravity wave drag parametrization.

The emphasis in the present paper was the stratospheric monthly mean circulation in the Northern Hemisphere during the winter season. The evaluation of the model performance during other seasons and the analysis of daily variability are in progress and will be reported later.

It was found that the December-January climatology of the observed zonal mean temperature and zonal wind is reasonably well simulated by the ECHAM3.5 model. The broad features of the zonal mean circulation are well captured by the model. For instance, in the lower stratosphere the simulation is characterized by weak winds and is dominated by quasi-stationary planetary waves. The tropospheric subtropical jets are clearly separated from and the zonal wind jets in the stratosphere, and the simulated and observed stratospheric zonal winds are of comparable strength. However, the simulated

stratospheric westerly winds do not show the equatorward tilt with height present in the observations. Associated with this polar confinement of the westerly stratospheric winds is a systematic cold bias in the polar lower stratosphere and upper troposphere, of about 5°-10°K.

The polar confinement of the winter stratospheric jet and the cold polar bias (related by means of the thermal wind equation) are problems common to other GCMs, see for instance Boville (1991) for the NCAR CCM1 model and Hamilton et al.(1994) for the GFDL SKYHI model. The most likely cause of these model deficiencies is an improper treatment of both resolved and unresolved gravity waves in low resolution GCMs. Some alleviation of the cold polar bias appears indeed to be achieved either by substantially increasing the horizontal resolution (Mahlman and Umscheid, 1987; Hamilton et al. 1994) or by including subgrid scale gravity wave drag (Boville, 1991). As far as the Northern Hemisphere is concerned, probably the consideration of orographic forcing only in a gravity wave drag parametrization may be sufficient. The imposed mesospheric drag at the upper boundary in the ECHAM3.5 simulation (a crude way to represent mesospheric subgrid scale gravity wave drag) in part corrects the magnitude of both the easterly and westerly stratospheric jets, thus improving the simulation of the upper and middle stratosphere. The imposed mesospheric drag however does not appear to affect the structure of the polar night jet in the early NH winter season. A recent review and discussion about the role of planetary and gravity waves in maintaining the general circulation of the stratosphere can be found in McIntyre (1992).

This study has also shown that a considerable amount of monthly interannual variability is present in the ECHAM3.5 simulation during the NH winter season in the stratosphere. Several aspects of the interannual variability have been examined, namely the interannual variability of the monthly mean, zonal mean circulation and the geographical distribution of variations in the monthly mean temperatures. It was found that both the NMC-CAC observations and the ECHAM3.5 simulation show a tendency for the interannual variability to be larger in January and, especially, in February than in December. In early winter, however, the simulated variability is underestimated in the lower stratosphere and upper troposphere. Given that in February the simulated interannual variability is generally comparable to that observed, the seasonal rate of increase of the variability is somewhat exaggerated in the model. It is interesting to note that the February simulation, when the model appears to be able to capture the kind of extreme variability present is the observations, is clearly distinguished from the December and January months, when extreme warm events do not occurs in the simulation. That a correct simulation of the interannual variability in early winter may be a more difficult task is also indicated by the results of Hamilton (1994).

The geographical distribution of the interannual variability of the December monthly mean temperature suggests that in the ECHAM3.5 model the dynamical processes responsible for the interannual variability may be inhibited by the model's polar cold

bias, somewhat more pronounced in early winter. Other reasons for the underestimation of the variability in the lower stratosphere and upper stratosphere may of course be related to deficiencies in the tropospheric simulation associated with the low horizontal resolution used.

An interesting and important point emerged from this work is that during February substantially different behaviors were obtained when the monthly interannual variability was computed from a 10-year sample of the simulation only. This results appears to be caused by the occurrence of two major warming type events during the first decade of the 20-year simulation, while none during the second decade, a result not in disagreement with observations. The fact that significant differences can occur between 10-year samples indicates that much longer integrations (quite probably even longer than the 20-years considered here) would be necessary for any firm conclusion concerning interannual variability.

Acknowledgements

The authors would like to thank William J. Randel for providing his compilation of the NMC-CAC global analyses and Christoph Brühl for providing the ozone distribution. Marco Giorgetta helped in modifying the Morcrette radiation scheme and computed Fig.2. Constructive discussions with Klaus Arpe, Kevin Hamilton and Jean-Jacques Morcrette, and the technical assistance of Ulrich Schlese and colleagues at DKRZ and MPI are gratefully acknowledged. Kevin Hamilton provided a copy of his unpublished papers.

Appendix

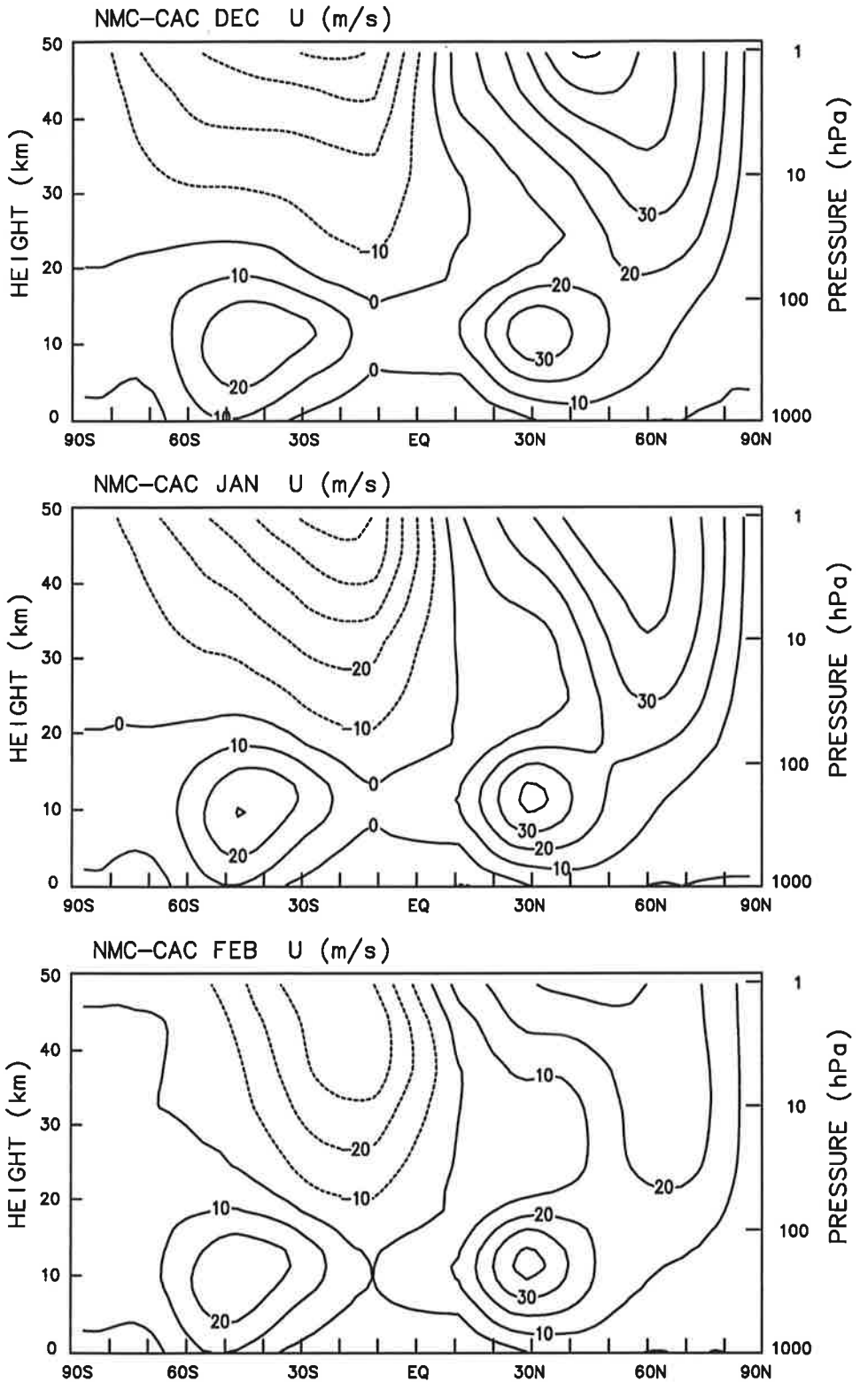

Figure A1 12-year NMC-CAC time average zonal mean zonal wind for December (upper panel); January (middle panel); and February (lower panel). Contour: 10 ms^{-1}.

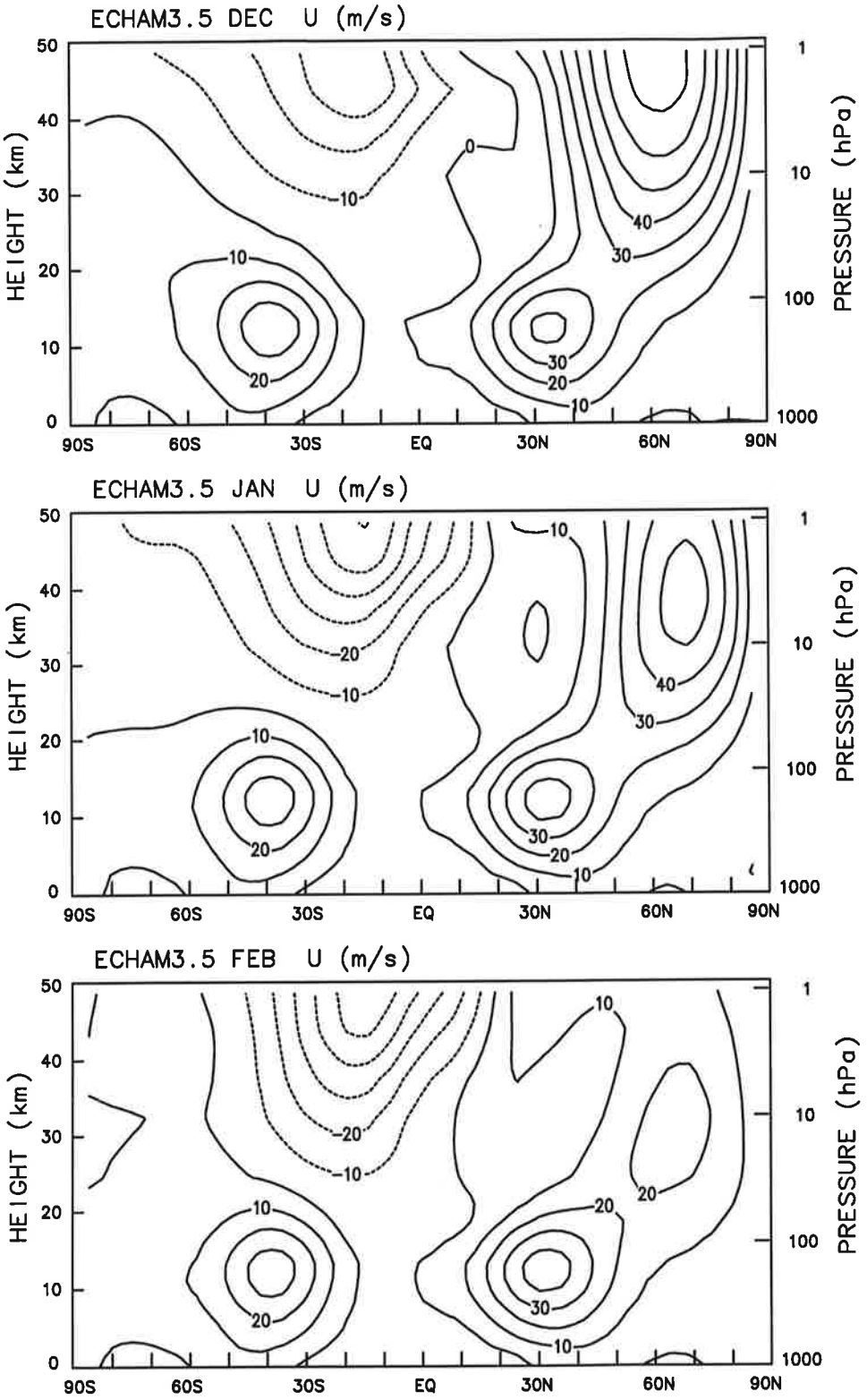

Figure A2 20-year ECHAM3.5 time average zonal mean zonal wind for December (upper panel); January (middle panel); and February (lower panel). Contour: 10 ms^{-1}.

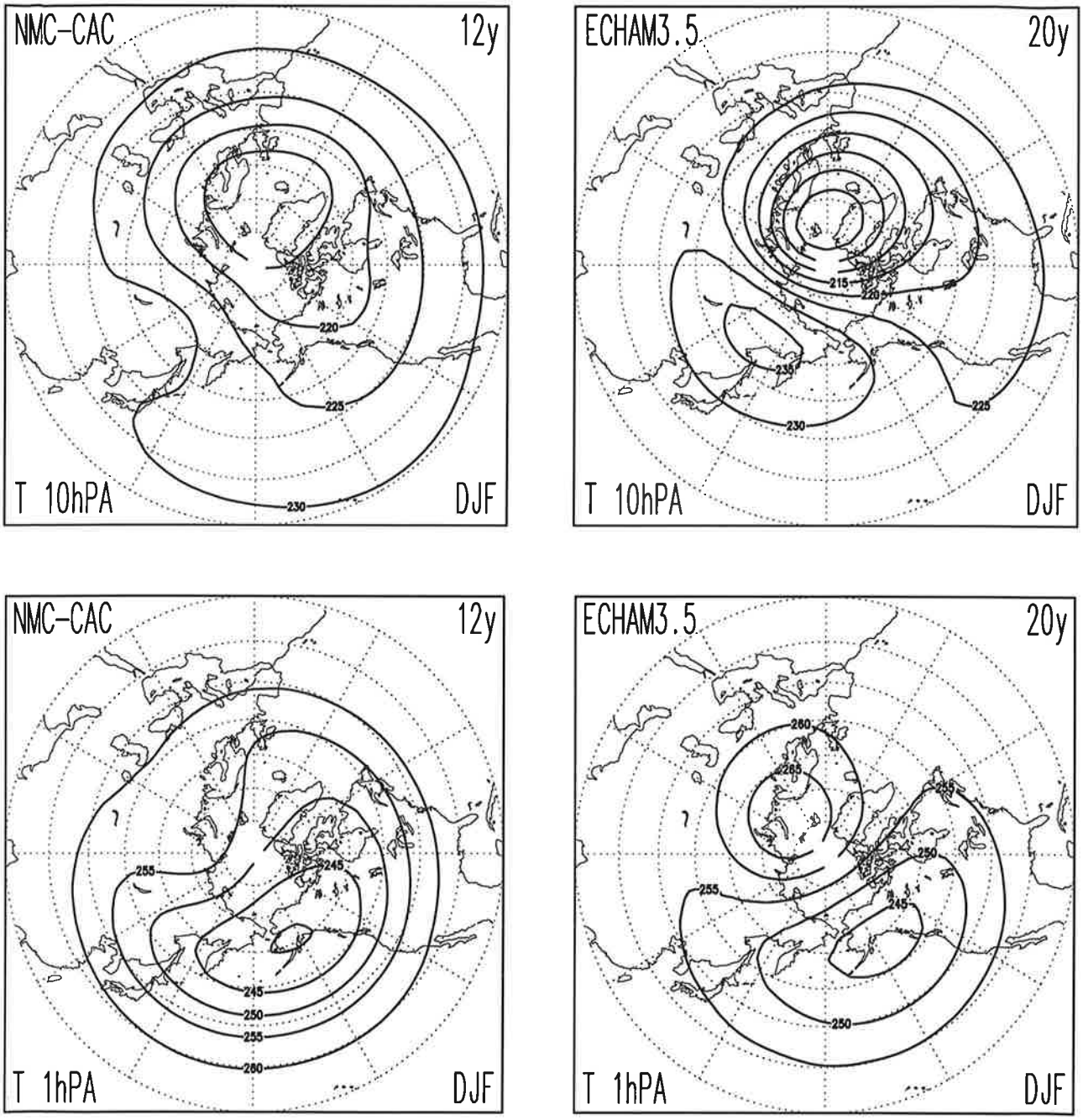

Figure A3 Northern Hemisphere DJF time average temperature at 10 hPa (upper panels) and at 1 hPa (lower panels) from the 12-year NMC-CAC observations (left column) and from the 20-year ECHAM3.5 simulation (right column). Contour: 5^{o} K.

References

Andrews, D. G., J. R. Holton and C. B. Leovy, 1987: Middle atmospheric dynamics. Academic press, 489 pp.

Blondin, C., 1989: Research on land surface parameterization schemes at ECMWF. *Proc. ECMWF workshop: Parameterization of fluxes over land surface*, 285-330.

Boville B. A., 1991: Sensitivity of simulated climate to model resolution. *J. Climate,* **4**, 469-485.

Boville, B. A. and W. J. Randel 1986: Observations and simulation of the variability of the stratosphere and troposphere in January. *J. Atmos. Sci.*, **43**, 3015-3034.

Brühl, C., 1993: Atmospheric effects of stratospheric aircraft. Report of the 1992 models and measurements workshop (Ed.s M. Prather and E. Remsberg). *NASA Reference Publication*, 1292 II.

Charney, J. G. and P. G. Drazin, 1961: Propagation of planetary-scale disturbances from the lower into the upper atmosphere. *J. Geophys. Res.*, **66**, 83-109.

Deque, M., C. Dreveton, A. Braun and D. Cariolle, 1994: The ARPEGE/IFS atmospheric model: A contribution to the French community climate modelling. *Climate Dynamics*, **10**, 249-266.

Farman, J. C., B. G. Gardiner and J. D. Shanklin, 1985: Large losses of total ozone in Antarctica reveal seasonal ClO_x/NOl_x interaction. *Nature,* **315,** 207-210.

Fels, S. B., 1976: Simple strategies for inclusion of Voigt effects in infrared cooling rate calculations. *App. Opt.*, **18**, 2634-2637.

Finger, F. G., M. E. Gelman, J. D. Wild, M. L. Chanin, A. Hauchecorne and A. J. Miller, 1993: Evaluation of NMC upper-stratospheric temperature analyses using rocketsonde and lidar data. *Bull. Am. Met. Soc.,* **74**, 789-798.

Dümenil, L. and E. Todini, 1992: A rainfall-runoff scheme for use in the Hamburg climate model. Advances in theoretical hydrology, a tribute to James Dooge (Ed. J. P. O'Cane). EGS *Series on Hydrological Sciences*, Elsevier Press. **1**, 129-157.

Gates, W. L., 1992: AMIP: The atmospheric model intercomparison project. *Bull. Am. Met. Soc.,* **73**, 1962-1970.

Geller, M. A., M-F. Wu and M. E. Gelman, 1983: Troposphere - stratosphere (surface-55 km) monthly winter general circulation statistics for the Northern Hemisphere. Four year averages, *J. Atmos. Sci.*, **40**, 1334-1352.

Geller, M. A., M-F. Wu and M. E. Gelman, 1984: Troposphere - stratosphere (surface-55 km) monthly winter general circulation statistics for the Northern Hemisphere. Interannual variations. *J. Atmos. Sci.*, **41**, 1726-1744.

Hamilton, K., 1994: Interannual variability in the Northern Hemisphere winter middle atmosphere in control and perturbed experiments with the GFDL SKY general circulation model. *J. Atmos. Sci.*, in press.

Hamilton, K., R. J. Wilson, J. D. Mahlman and L. J. Umscheid, 1994: Climatology of the SKYHI troposphere-stratosphere-mesosphere general circulation model. *J. Atmos. Sci.*, in press.

Labitzke, K., 1981: Stratospheric-mesospheric midwinter disturbances: A summary of observed characteristics. *J. Geophys. Res.*, **86,** 9665-9678.

Lau, N-C., 1992: Climate variability simulated in GCMs. Climate system modeling (Ed. K. E. Trenberth). Cambridge University Press, 617-642.

Lau, N-C. and M. J. Nath, 1987: Frequency dependence of the structure and temporal development of wintertime tropospheric fluctuation. Comparison of a GCM simulation with observations. *Mon. Wea. Rev.*, **115**, 251-271.

Laursen, L. and E. Eliasen, 1989: On the effects of the damping mechanisms in a atmospheric general circulation model. *Tellus*, **41A**, 385-400.

Louis, J. F., 1979: A parametric model of the vertical eddy fluxes in the atmosphere. *Boundary Layer Meteorology*, **17**, 187-202.

Mahlman, J. D. and L. J. Umscheid, 1987: Comprehensive modelling of the middle atmosphere: The influence of horizontal resolution. Transport Processes in the Middle Atmosphere (Ed.s G. Visconti and R. Garcia) Reidel, 251-266.

Matsuno, T., 1971: A dynamical model of the stratospheric sudden warming. *J. Atmos. Sci.*, **28**, 1479-1494.

McIntyre, M. E., 1992: Atmospheric dynamics: Some fundamentals, with observational implications. *Proc. Int. School Phys. "Enrico Fermi" CXV Course: The use of EOS for studies of atmospheric physics.* (Ed.s J. C. Gille and G. Visconti) North-Holland, 313-

386.

Mechoso, C. R., D.L. Hartmann and J. D. Farrara, 1985: Climatology and interannual variability of wave, mean-flow interaction in the southern hemisphere. *J. Atmos. Sci*, **42**, 2189-2206.

Morcrette, J. J., 1991: Radiation and cloud radiative properties in the European Centre for Medium Range Weather Forecasts forecasting system. *J. Geophys. Res.*, **96**, 9121-9132.

Morcrette J. J., L. Smith and Y. Fouquart, 1986: Pressure and temperature dependence of the absorption in longwave radiation parametrizations. *Betr. Phys. Atmosph.*, **59**, 455-469.

Naujokat, B., K. Labitzke, R. Lenschow, K. Petzoldt and R. C. Wohlfart, 1987: The stratospheric winter 1986/87: A major midwinter warming 35 years after they were first detected. *Beilage zur Berliner Wetterkarte,* **SO 9/87**, 16 pp.

Naujokat, B., K. Labitzke, R. Lenschow, K. Petzoldt and R. C. Wohlfart, 1988: The stratospheric winter 1987/88: An Unusually Early Major Midwinter Warming. *Beilage zur Berliner Wetterkarte,* **SO 6/88**, 20 pp.

Pawson, S., K. Labitzke, R. Lenschow, B. Naujokat, B. Rajewski, M. Wiesner and R.-C. Wohlfart, 1993: Climatology of the northern hemisphere stratosphere derived from Berlin analyses. Part 1: Monthly means. *Meteorol. Abhandlung*, neue Folge Serie A, Band 7 Heft 4, Verlag von Dietrich Reimer, 299 pp.

Ramaswamy, V., M. D. Schwarzkopf and K. P. Shine, 1992: Radiative forcing of climate from halocarbon-induced global stratospheric ozone loss. *Nature*, **355**, 810-812.

Randel, W. J., 1992: Global atmospheric circulation statistics, 1000-1 mb. *NCAR Technical Note TN-366+STR*, 256 pp.

Rasch, P. J., and D. L. Williamson, 1990: Computational aspect of moisture transport in global models of the atmosphere. *Quart. J. Roy. Meteor. Soc.*, **116**, 1017-1090.

Rind, D., R. Suozzo, N. K. Balachandran, 1988a: The GISS global climate middle atmosphere model. Part II: Model Variability due to interactions between planetary waves, the mean circulations, and gravity wave drag. *J. Atmos. Sci.*, **45**, 371-386.

Rind, D., R. Suozzo, N. K. Balachandran, A. Lacis and G. R. Russel, 1988b: The GISS global climate middle atmosphere model. Part I: Model structure and climatology. *J. Atmos. Sci.*, **45**, 329-370.

Roeckner, E., K. Arpe, L. Bengtsson, S. Brinkop, L. Dümenil, M. Esch, E. Kirk, F. Lunkeit, M. Ponater, B. Rockel, R. Sausen, U. Schlese, S. Schubert, W. Windelband, 1992: Simulation of the present-day climate with the ECHAM model: Impact of model physics and resolution. *MPI Report*, **93**, 172 pp.

Roeckner, E., M. Rieland, and E. Keup, 1991: Modelling of cloud and radiation in the ECHAM model. *Proc. ECMWF/WCRP workshop: Cloud, radiative transfer and the hydrological cycle*, 199-222.

Schwarzkopf, M. D. and S. B. Fels, 1991: The simplified exchange method revisited: An accurate, rapid method for computation of infrared cooling rates and fluxes. *J. Geophys. Res.*, **96**, 9075-9096.

Stolarski, R. S., P. Bloomfield and R. D. McPeters, 1991: Total ozone trends from Nimbus 7 TOMS data. *Geophys. Res. Let.*, **18**, 1915-1018.

Tiedtke, M., 1989: A comprehensive mass flux scheme for cumulus parametrization in large-scale models. *Mon. Wea. Rev.*, **117**, 1779-1800.